# Experimental results of radiation-driven, layered deuterium-tritium implosions with adiabat-shaped drives at the National Ignition Facility

V. A. Smalyuk, H. F. Robey, T. Döppner, D. T. Casey, D. S. Clark, O. S. Jones, J. L. Milovich, J. L. Peterson, B. Bachmann, K. L. Baker, L. R. Benedetti, L. F. Berzak Hopkins, R. Bionta, E. Bond, D. K. Bradley, D. A. Callahan, P. M. Celliers, C. Cerjan, K.-C. Chen, C. Goyon, G. Grim, S. N. Dixit, M. J. Eckart, M. J. Edwards, M. Farrell, D. N. Fittinghoff, J. A. Frenje, M. Gatu-Johnson, N. Gharibyan, S. W. Haan, A. V. Hamza, E. Hartouni, R. Hatarik, M. Havre, M. Hohenberger, D. Hoover, O. A. Hurricane, N. Izumi, K. S. Jancaitis, S. F. Khan, J. P. Knauer, J. J. Kroll, G. Kyrala, K. N. Lafortune, O. L. Landen, T. Ma, B. J. MacGowan, A. G. MacPhee, M. Mauldin, F. E. Merrill, A. S. Moore, S. Nagel, A. Nikroo, A. Pak, P. K. Patel, J. E. Ralph, D. B. Sayre, D. Shaughnessy, B. K. Spears, R. Tommasini, D. P. Turnbull, A. L. Velikovich, P. L. Volegov, C. R. Weber, C. C. Widmayer, and C. Yeamans

Citation: Phys. Plasmas **23**, 102703 (2016); doi: 10.1063/1.4964919

View online: http://dx.doi.org/10.1063/1.4964919

View Table of Contents: http://aip.scitation.org/toc/php/23/10

Published by the American Institute of Physics

# Experimental results of radiation-driven, layered deuterium-tritium implosions with adiabat-shaped drives at the National Ignition Facility

V. A. Smalyuk,[1] H. F. Robey,[1] T. Döppner,[1] D. T. Casey,[1] D. S. Clark,[1] O. S. Jones,[1] J. L. Milovich,[1] J. L. Peterson,[1] B. Bachmann,[1] K. L. Baker,[1] L. R. Benedetti,[1] L. F. Berzak Hopkins,[1] R. Bionta,[1] E. Bond,[1] D. K. Bradley,[1] D. A. Callahan,[1] P. M. Celliers,[1] C. Cerjan,[1] K.-C. Chen,[2] C. Goyon,[1] G. Grim,[1] S. N. Dixit,[1] M. J. Eckart,[1] M. J. Edwards,[1] M. Farrell,[2] D. N. Fittinghoff,[1] J. A. Frenje,[3] M. Gatu-Johnson,[3] N. Gharibyan,[1] S. W. Haan,[1] A. V. Hamza,[1] E. Hartouni,[1] R. Hatarik,[1] M. Havre,[2] M. Hohenberger,[4] D. Hoover,[2] O. A. Hurricane,[1] N. Izumi,[1] K. S. Jancaitis,[1] S. F. Khan,[1] J. P. Knauer,[4] J. J. Kroll,[1] G. Kyrala,[5] K. N. Lafortune,[1] O. L. Landen,[1] T. Ma,[1] B. J. MacGowan,[1] A. G. MacPhee,[1] M. Mauldin,[2] F. E. Merrill,[5] A. S. Moore,[1] S. Nagel,[1] A. Nikroo,[1] A. Pak,[1] P. K. Patel,[1] J. E. Ralph,[1] D. B. Sayre,[1] D. Shaughnessy,[1] B. K. Spears,[1] R. Tommasini,[1] D. P. Turnbull,[1] A. L. Velikovich,[6] P. L. Volegov,[5] C. R. Weber,[1] C. C. Widmayer,[1] and C. Yeamans[1]

[1]*Lawrence Livermore National Laboratory, Livermore, California 94550, USA*
[2]*General Atomics, San Diego, California 92186, USA*
[3]*Plasma Science and Fusion Center, Massachusetts Institute of Technology, Cambridge, Massachusetts 02139, USA*
[4]*Laboratory for Laser Energetics, University of Rochester, Rochester, New York 14623, USA*
[5]*Los Alamos National Laboratory, Los Alamos, New Mexico 87545, USA*
[6]*Naval Research Laboratory, Washington, DC 20375, USA*

(Received 11 July 2016; accepted 26 September 2016; published online 17 October 2016)

Radiation-driven, layered deuterium-tritium (DT) implosions were carried out using 3-shock and 4-shock "adiabat-shaped" drives and plastic ablators on the National Ignition Facility (NIF) [E. M. Campbell *et al.*, AIP Conf. Proc. **429**, 3 (1998)]. The purpose of these shots was to gain further understanding on the relative performance of the low-foot implosions of the National Ignition Campaign [M. J. Edwards *et al.*, Phys. Plasmas **20**, 070501 (2013)] versus the subsequent high-foot implosions [T. Döppner *et al.*, Phys. Rev. Lett. **115**, 055001 (2015)]. The neutron yield performance in the experiment with the 4-shock adiabat-shaped drive was improved by factors ∼3 to ∼10, compared to five companion low-foot shots despite large low-mode asymmetries of DT fuel, while measured compression was similar to its low-foot companions. This indicated that the dominant degradation source for low-foot implosions was ablation-front instability growth, since adiabat shaping significantly stabilized this growth. For the experiment with the low-power 3-shock adiabat-shaped drive, the DT fuel compression was significantly increased, by ∼25% to ∼36%, compared to its companion high-foot implosions. The neutron yield increased by ∼20%, lower than the increase of ∼50% estimated from one-dimensional scaling, suggesting the importance of residual instabilities and asymmetries. For the experiment with the high-power, 3-shock adiabat-shaped drive, the DT fuel compression was slightly increased by ∼14% compared to its companion high-foot experiments. However, the compression was reduced compared to the lower-power 3-shock adiabat-shaped drive, correlated with the increase of hot electrons that hypothetically can be responsible for reduced compression in high-power adiabat-shaped experiments as well as in high-foot experiments. The total neutron yield in the high-power 3-shock adiabat-shaped shot N150416 was $8.5 \times 10^{15} \pm 0.2 \times 10^{15}$, with the fuel areal density of $0.90 \pm 0.07$ g/cm$^2$, corresponding to the ignition threshold factor parameter IFTX (calculated without alpha heating) of $0.34 \pm 0.03$ and the yield amplification due to the alpha heating of $2.4 \pm 0.2$. The performance parameters were among the highest of all shots on NIF and the closest to ignition at this time, based on the IFTX metric. The follow-up experiments were proposed to continue testing physics hypotheses, to measure implosion reproducibility, and to improve quantitative understanding on present implosion results. *Published by AIP Publishing.* [http://dx.doi.org/10.1063/1.4964919]

## I. INTRODUCTION

The goal of inertial confinement fusion (ICF)[1–3] is to implode a spherical target to compress deuterium-tritium (DT) fuel and achieve high temperature in a central hot spot, to trigger ignition of the DT fuel. During the National Ignition Campaign (NIC) on the National Ignition Facility (NIF),[4] the highest compression of DT fuel was achieved in implosions with an areal density of $\rho R \sim 1.2$ g/cm$^2$.[5] These implosions were driven with ∼1.6 MJ "low-foot" (LF) laser pulses at a peak power of ∼336 TW, achieving peak implosion velocities of ∼320 km/s,[5–7] and the temperatures and

neutron yields were significantly lower than expectations. In the lowest-yield implosions, the performance was correlated with a presence of the plastic ablator material mixed into the DT hot spot showing the detrimental effects of hydrodynamic instabilities.[8,9] In recent x-ray radiography experiments, it was found that ablation-front hydrodynamic instabilities including Richtmyer-Meshkov (RM)[10,11] and Rayleigh-Taylor (RT)[12,13] instabilities had larger than expected initial seeds, probably contributing to the poor implosion performance during NIC.[14–16] The capsule support "tent" also has been found to seed significant instability growth,[16,17] also affecting performance during NIC.

Recent "high-foot" (HF) experiments[18–23] on NIF have shown much-improved neutron yield performance compared to LF. These HF implosions employed a higher radiation temperature during the early stage of the drive to launch a stronger first shock into the capsule.[18] As a result, the stability at the outer ablation surface of the capsule was improved[24] by putting the capsule on a higher adiabat $\alpha$.[7] The adiabat $\alpha$ is generally the ratio of the pressure to the minimum Fermi-degenerate pressure. For specific quantitative evaluation of the fuel adiabat, we use a definition based on mass-averaged entropy as described in Ref. 7. Improving ablation-front stability for NIF indirect-drive implosions was discussed and proposed at the Workshop on the Science of Fusion Ignition on NIF in 2012.[25] Significant instability stabilization was experimentally observed in HF drives, compared to LF drives, in Hydrodynamic Growth Radiography (HGR) experiments.[26–30] In these implosions, the instability growth was measured using time-resolved x-ray radiography of large-amplitude, two-dimensional (2-D) modulations.[26–30] Strong instability stabilization at ablation-front in the HF drive was correlated with $\sim 2\times$ temperature increase and $\sim 10\times$ neutron yield increase in layered DT implosions.[18–23] However, this stability improvement came at the expense of ultimate compressibility due to the higher DT adiabat. As a result, the HF drive resulted in fuel compression of only $\rho R \sim 0.8\,\mathrm{g/cm^2}$ ($\alpha \sim 2.4$) compared to $\sim 1.2\,\mathrm{g/cm^2}$ ($\alpha \sim 1.5$) for the LF drive.

While high compression was achieved in LF experiments and yield multiplication due to alpha heating was demonstrated in HF experiments, many physics questions about causes of performance degradation still remain. Some of the main questions include quantitative understanding of the impact of hydrodynamic instabilities, low-mode asymmetries, compression, and fuel preheat on implosion performance in HF and LF implosions. The "adiabat-shaping" (AS) campaign was designed and performed to get insights into this physics.[31–38] To understand the role of the ablation-front instabilities in the high-compression LF implosions, a 4-shock "adiabat-shaped" (4-shock AS) drive was designed to improve ablation-front stability while keeping fuel adiabat and compression at the same high level as in 4-shock LF drives.[31,33–36,38] To understand the role of the compression in implosion performance, a 3-shock "adiabat-shaped" (3-shock AS) drive was designed to moderately improve fuel compression relative to HF drives, while keeping the ablation-front stability at the same level as in 3-shock HF drives.[31,32,37,38]

Adiabat-shaped (AS) drives were developed for indirect drive[31–33] based on works by Clark *et al.*,[31] Milovich *et al.*,[33] and Peterson *et al.*[32] The efficacy of these AS designs for indirect drive was demonstrated in shock propagation ("key-hole") experiments.[34,38] Post-shot simulations of those experiments showed that in the 3-shock AS design, the fuel adiabat was reduced slightly ($\sim$10%) from the nominal $\alpha \sim 2.3$ used in the HF.[34,38] In the 4-shock adiabat shaped design, the fuel adiabat $\alpha \sim 1.6$ was similar to that in LF.[34,38] The ablation-front stability was measured in hydrodynamic growth radiography (HGR) experiments.[35,37] It was shown that the stability of the 3-shock AS drive was comparable to the HF drives.[37] In the experiments with the 4-shock AS drive, the stability was significantly improved relative to the LF drives, but not yet to the level of the HF, especially for high modes >90.[35] First results of the adiabat-shaped layered DT implosions were presented in Refs. 36–38. This article extends this work by showing all the experimental results in these adiabat-shaped layered DT implosions, not presented in earlier publications.[36–38] The new information includes capsule and DT layer parameters and roughnesses; measured hot-spot neutron and x-ray shapes and their asymmetries; fuel compression and shell areal-density nonuniformities; ablator hot-spot mix; hot-electron signals; and inferred performance parameters such as hot-spot pressure, ignition threshold factor parameter IFTX, Lawson parameter Generalized Lawson Criterion (GLC), and yield amplification due to alpha heating.

The details of adiabat-shaped laser drives are described in Sec. II, while the concept of adiabat-shaping is reviewed in Sec. III. Target details including capsule ablator and DT layer roughnesses are presented in Section IV. The neutron performance results are shown in Sec. V. Hot-spot x-ray shapes and asymmetries are described in Sec. VI. Neutron hot-spot images and DT fuel compression are presented in Sec. VII. Fuel areal-density non-uniformities at peak compression are presented in Sec. VIII. Measurements of the ablator mix into the hot-spot are shown in Sec. IX. Hot-electron measurements are described in Sec. X. The experimental measurements along with inferred performance parameters are discussed in Sec. XI. Future experiments are discussed in Sec. XII. Summary and conclusions are presented in Sec. XIII.

## II. DRIVE DETAILS

Figures 1–3 show details of the details of the adiabat-shaping pulse shapes used in layered DT implosions experiments and compare them to companion LF and HF pulses from which they were derived. Figure 1(a) shows the laser pulse used in the layered DT implosion with 4-shock AS (shot N141123), compared to the LF drive (shot N120321 (Ref. 5)) used in implosions with similar laser powers, energies, and implosion velocities of $\sim$320 km/s. The pulses for 4-shock AS and LF drives were at a peak power of $\sim$340 TW and the total energy of $\sim$1.6 MJ, as shown in Table I. Corresponding ablation-front instability growth factors (GFs) at peak velocity are shown in Fig. 1(b) and compared to the HF drive (shot N130812 (Ref. 18)), described in

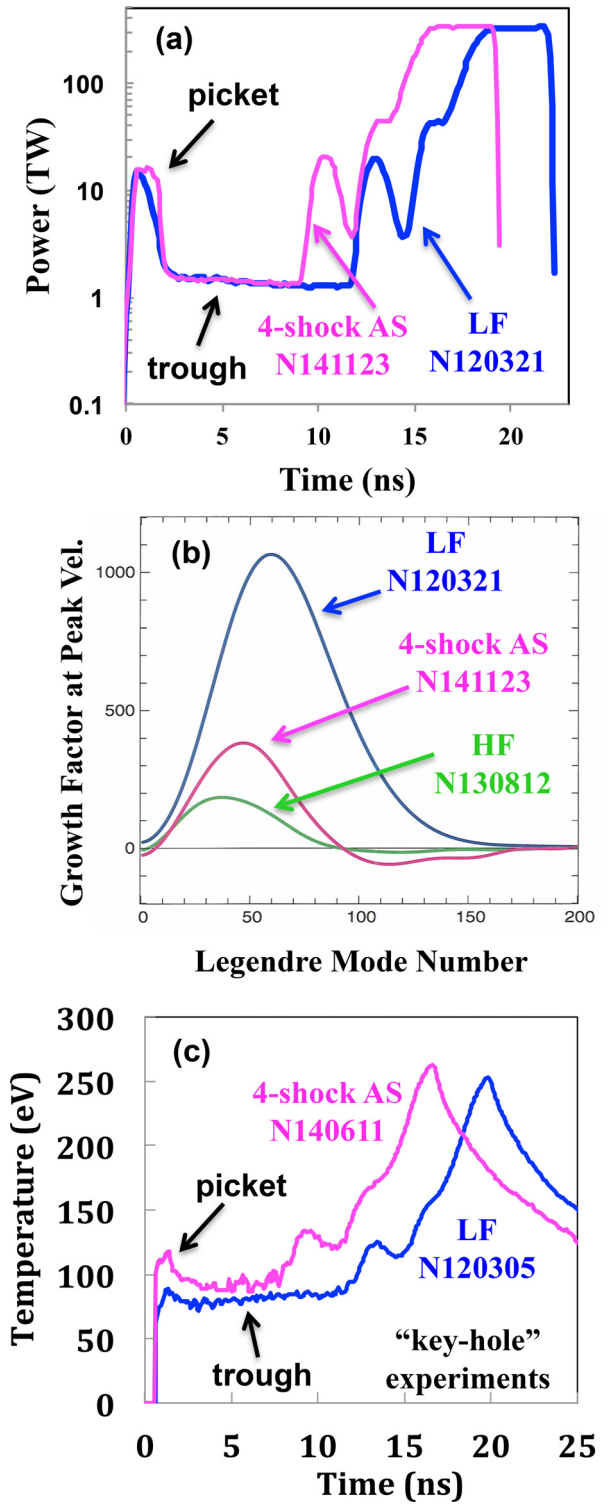


FIG. 1. (a) Laser power vs time for LF and 4-shock AS drives. Regions of the pickets and trough are indicated. (b) Predicted amplitude modulation growth factors at peak velocity as a function of modulation Legendre mode number for LF, 4-shock AS drives, compared to HF shot N130812, driven at similar implosion velocities. (c) Radiation drive temperature vs time for LF and 4-shock AS experiments as measured in tuning "key-hole" shots to develop ~330 TW drives. While the radiation temperature stays relatively constant during the trough in the LF drive, it gradually decreases in the 4-shock AS drive, indicating reduced first shock heating as it propagates toward the inner capsule surface.

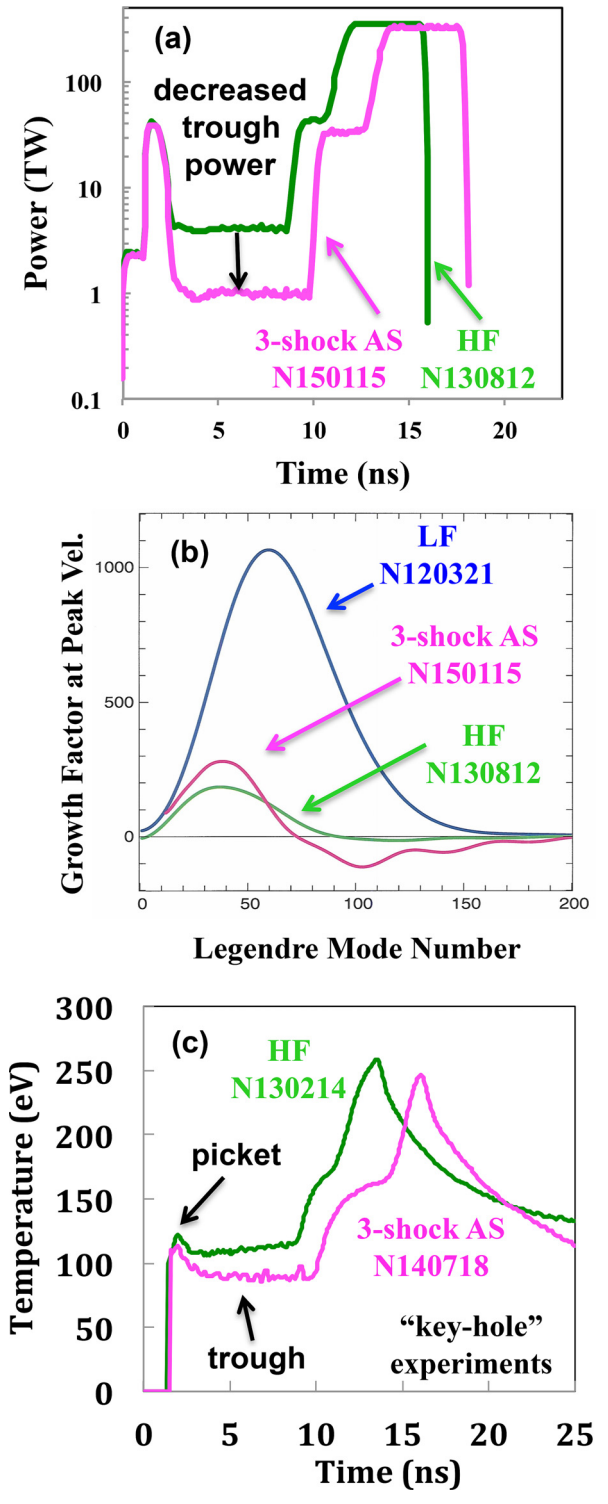


FIG. 2. Laser power vs time for HF and 3-shock AS drives. (b) Predicted amplitude modulation growth factors at peak velocity as a function of modulation Legendre mode number for LF, 3-shock AS, and HF drives, driven at similar implosion velocities. (c) Radiation drive temperature vs time for HF and 3-shock AS drives as measured in tuning "key-hole" shots to develop ~340 TW drives. While the radiation temperature stays relatively constant during the trough in the HF drive, it gradually decreases in the 3-shock AS drive, indicating reduced first shock heating as it propagates toward the inner capsule surface.

Fig. 2. Comparing the 4-shock AS pulse with its companion LF pulse, one can see that the principal change was an increase of the energy in the first picket energy from 15 kJ to 23 kJ at the same picket power of ~15 TW as in LF. The trough power was kept at the same level of ~1.5 TW as in LF pulse, while the main part of the pulse (starting with a second picket) was advanced by ~2.7 ns to compensate for a

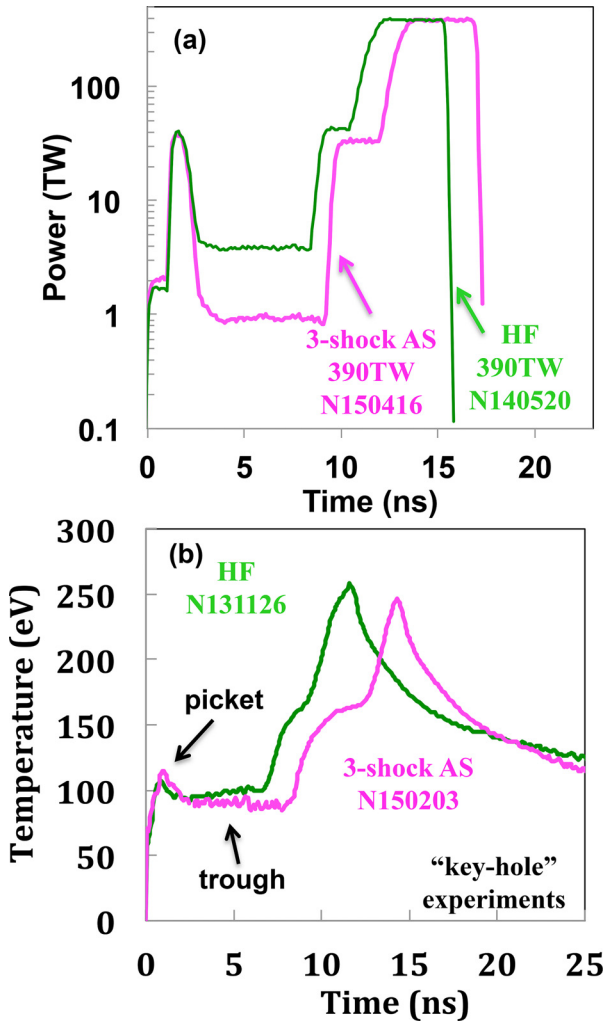


FIG. 3. (a) Laser power vs time for high-power HF and high-power 3-shock AS drives, driven at similar implosion velocities. (b) Radiation drive temperature vs time for HF and 3-shock AS drives as measured in tuning "key-hole" shots to develop ~390 TW drives. While the radiation temperature stays relatively constant during the trough in the HF drive, it gradually decreases in the 3-shock AS drive, indicating reduced first shock heating as it propagates toward the inner capsule surface.

TABLE I. Key experimental results for the 4-shock AS shot N141123, 3-shock AS shot N150115, and high-power 3-shock AS shot N150416.

| | N141123 | N150115 | N150416 |
|---|---|---|---|
| Pulse name, peak power | 4-sh AS, 339 TW | 3-sh AS, 328 TW | 3-sh AS, 388 TW |
| Hohlraum | DU | DU | DU |
| Ablator dopant | 1 × Si | 1 × Si | 1 × Si |
| Energy (MJ] | 1.60 ± 0.05 | 1.58 ± 0.05 | 1.74 ± 0.05 |
| Radiation drive temperature (eV) | 289[a] ± 4 | 289 ± 4 | 303 ± 4 |
| Capsule outer radius ($\mu$m) | 1120.4 ± 1.0 | 1126.8 ± 1.0 | 1104.7 ± 1.0 |
| Ablator shell thickness ($\mu$m) | 194.0 ± 0.2 | 196.0 ± 0.2 | 175.0 ± 0.2 |
| DT ice layer thickness ($\mu$m) | 69.5 ± 0.3 | 69.3 ± 0.3 | 70.6 ± 0.2 |
| Effective groove rms K ($\mu$m) | 0.75 ± 0.3 | 1.20 ± 0.5 | 0.70 ± 0.3 |
| Larger groove area ($\mu m^2$) | 200 ± 100 | 1000 ± 200 | 200 ± 100 |
| Tent thickness (nm) | 31.0 ± 0.5 | 33.0 ± 0.5 | 29.0 ± 0.5 |
| Experimental results | | | |
| Total yield ($10^{15}$) | 1.37 ± 0.02 | 3.77 ± 0.13 | 8.46 ± 0.19 |
| Ti (keV) | 3.40 ± 0.15 | 3.98 ± 0.14 | 5.36 ± 0.18 |
| DSR (%) | 5.45 ± 0.19 | 5.04 ± 0.35 | 4.65 ± 0.32 |
| X-ray bang time (ns) | 19.81 ± 0.02 | 18.67 ± 0.10 | 17.53 ± 0.02 |
| X-ray burn width (ps) | 108 ± 13 | 126 ± 15 | 118 ± 11 |
| Nuclear burn width (ps) | 141 ± 30 | 138 ± 30 | 128 ± 30 |
| Laser energy coupling (%) | 87 ± 3 | 83 ± 5 | 86 ± 5 |
| SBS backscatter (kJ) | 48 ± 11 | 29 ± 16 | 36 ± 9 |
| SRS backscatter (kJ) | 157 ± 52 | 236 ± 72 | 211 ± 77 |
| Shell optical-depth at 10.9 keV | 1.69 ± 0.40 | 1.13 ± 0.40 | 0.74 ± 0.30 |
| DT fuel $\rho$R (g/cm$^2$) | 1.05 ± 0.04 | 0.97 ± 0.07 | 0.90 ± 0.07 |
| Estimated ablator $\rho$R (g/cm$^2$) | 0.58 ± 0.20 | 0.36 ± 0.10 | 0.21 ± 0.07 |
| Estimated total $\rho$R (g/cm$^2$) | 1.63 ± 0.20 | 1.33 ± 0.12 | 1.11 ± 0.10 |
| Primary neutron P0 ($\mu$m) | 25.7 ± 2.0 | 29.4 ± 1.7 | 27.9 ± 1.6 |
| Primary neutron P2/P0 (%) | −32 ± 4 | −11 ± 4 | 0 ± 6 |
| X-ray P0 ($\mu$m) | 23.6 ± 4.1 | 28.1 ± 1.1 | 27.6 ± 1.2 |
| X-ray P2/P0 (%) | −2.6 ± 5.4 | −3.1 ± 2.4 | −6.3 ± 2.0 |
| X-ray P4/P0 (%) | 6.1 ± 3.0 | −6.0 ± 1.7 | 5.6 ± 0.8 |
| X-ray M0 ($\mu$m) | 26.6 ± 1.6 | 29.8 ± 1.1 | 30.4 ± 1.2 |
| X-ray M2/M0 (%) | 15.0 ± 2.7 | 4.6 ± 1.1 | 10.1 ± 1.5 |
| X-ray M4/M0 (%) | 4.6 ± 0.6 | 6.2 ± 1.1 | 4.3 ± 1.2 |
| Inferred quantities | | | |
| Hot spot pressure (Gbar) | 153 ± 20 | 168 ± 18 | 210 ± 22 |
| Ps (atm s) | 16.3 ± 2.1 | 20.7 ± 2.2 | 24.1 ± 2.5 |
| ITFX with $\alpha$ heating | 0.17 ± 0.01 | 0.42 ± 0.06 | 0.81 ± 0.12 |
| ITFX without $\alpha$ heating | 0.12 ± 0.01 | 0.23 ± 0.02 | 0.34 ± 0.03 |
| Yield amplification from ITFX | 1.47 ± 0.04 | 1.86 ± 0.11 | 2.42 ± 0.19 |
| GLC with $\alpha$ heating from ITFX | 0.46 ± 0.02 | 0.68 ± 0.05 | 0.91 ± 0.06 |
| GLC with $\alpha$ heating from P$\tau$ | 0.34 ± 0.04 | 0.59 ± 0.06 | 1.16 ± 0.10 |

[a]Measured in the equivalent plastic-shell implosion.

stronger first shock launched by the stronger first picket and to allow all shocks to merge at the same location in the DT fuel. In simulations,[33,38] the small increase of ~8 kJ in the picket energy in the 4-shock AS pulse had a strong effect on ablation-front stability, while the same trough power provided the similar adiabat and compression of the DT fuel as in the LF pulse. As shown in Fig. 1(b), the calculated peak growth factor was reduced by ~3 times with adiabat-shaping, compared to the LF pulse; however, the calculated reduction was less than that with the HF drive (~5 times). Radiation drive temperatures vs time for LF and 4-shock AS experiments are shown in Fig. 1(c). These measurements were performed in tuning "key-hole" shots[34] used to develop ~330 TW drives. The drive x-ray temperatures were measured with a Dante detector.[39] While the radiation temperature stays relatively constant during the trough in the LF drive, it gradually decreases in the 4-shock AS drives, indicating reduced first shock heating as it propagates toward the inner capsule surface which is the main signature of adiabat shaping.

Figure 2(a) shows the laser pulse used in the layered DT implosion with 3-shock AS (shot N150115), compared to its companion HF drive (shot N130812). The pulse for the 3-shock AS drive was at a peak power of ~330 TW and the total energy of ~1.6 MJ. The pulse for the HF drive used a slightly higher power of ~350 TW and a laser energy of ~1.7 MJ to compensate for the fact that it was used with a slightly less efficient gold enclosure around the capsule, or hohlraum, compared to the uranium hohlraum used in the shots with AS drives, shown in Table I. The 3-shock AS

pulse was derived from the HF pulse with a principal change being a decrease of trough power from 4 TW to 1 TW, while the first picket energy was kept the same, ~38 kJ. The main part (starting with a second picket) of the pulse was delayed by ~2 ns to compensate for a longer propagation time of the first decaying shock. The second picket was slightly reduced, in addition to lower trough, resulting in the lower predicted DT fuel adiabat by ~10%, compared to the HF drive. As shown in Fig. 2(b), the predicted peak ablation-front growth factor at peak velocity was reduced by ~4 times with adiabat-shaping, compared to the LF pulse, and comparable to the reduction in the HF drive, while compression was increased, as described below. Figure 2(c) shows radiation drive temperatures vs time for HF and 3-shock AS experiments. These measurements were performed in tuning "key-hole" shots[34] used to develop ~340 TW drives. While the radiation temperature stayed relatively constant during the trough in the HF drive, it gradually decreased in the 3-shock AS drive.

Figure 3(a) shows the laser pulse used in the high-power layered DT implosion with 3-shock AS (shot N150416), compared to a companion HF drive (shot N140520 (Ref. 23)). The pulse for the high-power 3-shock AS drive was at a peak power of ~390 TW, total energy of ~1.7 MJ, and similar to its companion HF shot N140520, as shown in Table I. Figure 3(b) shows radiation drive temperatures vs time for HF and 3-shock AS experiments performed in tuning "key-hole" shots[34] used to develop high-power ~390 TW drives. While the radiation temperature stays relatively constant during the trough in the HF drive, it gradually decreases in the 3-shock AS drives, similar to the lower power drives, shown in Figs. 1 and 2. Predicted peak ablation-front growth factors at peak velocity were increased by ~2× for both high-power AS and HF shots, compared to the ~330-TW AS and HF shots [shown in Fig. 2(b)], respectively. The drive x-ray fluxes were measured with a Dante detector for these shots.[39] The inferred peak radiation temperatures were $289 \pm 4$ eV for both ~330-TW 4-shock and 3-shock AS shots. The peak radiation temperature was higher, $303 \pm 4$ eV, for the ~390-TW 3-shock AS shot, as shown in Table I.

As shown in Table I, the laser energy coupling for the adiabat-shaped shots was around ~85%. The backscatter was primarily due to Stimulated Raman Scattering (SRS) with a lower contribution due to Stimulated Brillouin Scattering (SBS).[38] Both SRS and SBS peaked during the high-power parts of the laser pulses.[38] The energy couplings in adiabat-shaped experiments were similar to LF and HF experiments.

## III. ADIABAT SHAPING

Adiabat shaping in ICF generally means setting the ablator on a higher adiabat than the DT fuel. The high adiabat $\alpha$ of the ablator leads to higher ablation velocity, which stabilizes the RT instability, whereas the low adiabat of the fuel permits its effective compression, thereby improving the performance of an adiabat-shaped target compared to the one characterized by a single value of $\alpha$. The target adiabat can be shaped by different methods, including propagation of decaying shock wave(s) driven by "picket fence" laser pulses, target preheat by the x rays from a thin high-Z film on its surface, or density stratification in the ablator material (e.g., foam-plastic layers). The concept of adiabat-shaping was first published by Bodner *et al.*[40] It was advanced with the direct drive on OMEGA,[41–44] using both "decaying shock"[41,43] and "density gradient relaxation"[43] techniques. In the decaying shock concept, a strong shock produced by a laser picket heats the outer region of the ablator, putting it on a higher adiabat $\alpha$. During acceleration, the higher ablator $\alpha$ leads to higher ablation velocity, which stabilizes the RT instability, in the OMEGA direct-drive designs. When the pre-pulse switches off, the shock is no longer supported and decays as it travels toward the capsule's inner surface, resulting in reduced $\alpha$ in the fuel, allowing high compression of the DT fuel.[41] In earlier direct-drive designs, "tailored density profiles"[45] were proposed to stabilize Richtmyer-Meshkov (RM) oscillations[46–49] to reduce initial modulations, or "seeds," for subsequent RT growth, after such a technique was proposed in Z-pinches.[50]

In the indirect drive, adiabat-shaping was developed based on works by Clark *et al.*[31] and Peterson *et al.*[32] Clark *et al.* have shown that the seed for the exponential RT growth can be controlled primarily by the strength of the first picket, while it is roughly independent of the trough [see picket and trough as indicated in Fig. 1(a)]. On the other hand, the fuel adiabat is almost exclusively determined by the trough level and is largely independent of the first picket. Therefore, the picket and the trough levels provide two independent "knobs" that can be used to control separately the RT seeding and fuel adiabat in the indirect drive. In contrast to the direct-drive case, the adiabat-shaping pulses in the indirect drive control the perturbation evolution during the first shock transit to optimize primarily the ablative RM instability phase, not the RT instability.[35]

Increased laser drive early in the pulse increases the ablation pressure during shock transit through the shell. This increases the ablative RM oscillation frequency and the magnitude of ablative stabilization before the onset of the RT growth.[41,46–49] For indirect drive adiabat-shaping designs, modes near the peak of the ablative RT growth rate undergo ~1 RM oscillation prior to RT amplification.[31,32,35,51] The net effect is that low mode numbers experience positive growth and high numbers experience negative growth, and the mode number of the node undergoing zero growth scales inversely with the strength of the first shock. Therefore, it is possible to reduce the overall effect of instability growth by placing the zero RM growth node near the peak of the RT growth. For example, the zero RM growth node was predicted to be near mode ~90 in the 4-shock AS design, while it is located at higher mode ~160 in the LF design, as shown in Fig. 1(b). This prediction was confirmed in recent HGR experiments[35] and in earlier HGR experiments.[32]

The relative locations of the zero-growth nodes can be understood in terms of ablative RM instability[41] as applied to indirect drive implosions.[32,51,52] The amplitude of any modulation at the outer capsule surface with wavenumber of $k$ will evolve after the launch of the first shock. The modulation can grow, and then decay and even reverse its phase due

to the ablative RM oscillations before second shock launch. The modulation amplitude growth factor $\eta(k)$ can be approximated as follows:[51,53]

$$\eta(\mathrm{k}) \approx \frac{\mathrm{C}_s}{\sqrt{V_{bl}V_a}}\,\mathrm{e}^{-2kV_at}\,\mathrm{f}(C)\sin\left(k\sqrt{V_{bl}V_a}t+0.3\right) - \frac{\mathrm{C}_s}{V_{bl}}\,\mathrm{g}(\mathrm{C})\sin\left(1.1\sqrt{C/3}kV_at+1\right), \quad (1)$$

where $\mathrm{C}_s$ is the post-shock sound speed, $V_a$ is the ablation velocity, $V_{bl}$ is the $k$ dependent blow-off velocity $V_{bl} = \frac{V_a}{\left(2.4\frac{kL}{\nu}\right)^{1/\nu}}$, $L$ is the ablation front width, $\nu$ is the thermal conductivity exponent, $C$ is the first shock compression ratio, and $t$ is the time before second shock launch. Equation (1) shows that ablation-front modulations oscillate in time due to the dynamic overpressure damped by the ablation [first term including $\mathrm{e}^{-2kV_at}$ in the right-hand side of Eq. (1)] and the convection of the shock-induced vorticity [second term in the right-hand side of Eq. (1)]. Setting Eq. (1) to 0, and recognizing that the sine term values are near 1 at the mode number node $l_0$ we arrive at[52]

$$l_0 \approx \frac{R\ln\left[\left(2.1/(C-1)^{0.9}\right)(R\nu/2.4l_0L)^{\frac{1}{2\nu}}\right]}{2V_at}, \quad (2)$$

where $R$ is the average capsule outer radius up to the time of the second shock launch. The estimated RM node numbers, based on this model and Eq. (2), were $l_0 \approx 85$ and $l_0 \approx 63$, for the 4-shock AS drive and 3-shock AS drive, respectively.[52] For the HF and LF drives, the estimated RM node numbers were $l_0 \approx 65$ and $l_0 \approx 116$, respectively.[52] The estimated node numbers are in reasonable agreement with the simulated node numbers for all four drives, as shown in Figs. 1(b), and 2(b).

## IV. CAPSULE ABLATOR AND DT LAYER

Spherical targets with outer plastic shells and inner cryogenic DT layers were imploded using x-ray drive produced in Au-lined uranium hohlraums on the National Ignition Facility (NIF)[4] in these adiabat-shaping experiments. Table I shows details of the capsules and DT layers used in these implosions. Plastic shells including Si-doped layers had an inner cryogenic DT layer with a nominal thickness of ~69 $\mu$m. For two mid-power (~330-TW) drive experiments, the capsule had nominal ~195-$\mu$m thicknesses and ~2260-$\mu$m-initial outer diameters, while the thinner, ~175 $\mu$m thick, capsule was used for the high-power (~390 TW) 3-shock AS shot N150416. Capsule and hohlraum details were shown in Refs. 5 and 18, with the exceptions that the hohlraums were made with uranium with a 0.6 $\mu$m-thick gold lining. The U produces higher drive at peak power. The inner Au layer provides oxidation protection for the U, as well as ensuring laser deposition in Au, and higher x-ray drive at early times in the x-ray drive. The nominal thickness of the support membrane (tent) was ~30 nm in all three experiments.

The roughnesses of the plastic capsule surfaces were comprehensively characterized. Figure 4 shows the initial measured power spectrum of the capsules' outer-surface roughness as a function of mode number compared to the NIF specification used in the 4-shock AS DT implosion. In all three AS shots, the initial surface roughness powers were similar and slightly better than the NIF specifications. Figure 5 shows the power spectra of the DT ice layer roughness as a function of mode number measured in three perpendicular views and compared to the NIF specification for the 4-shock AS DT implosion. For all three shots, the measured power spectra of the ice roughness were better than NIF specifications.

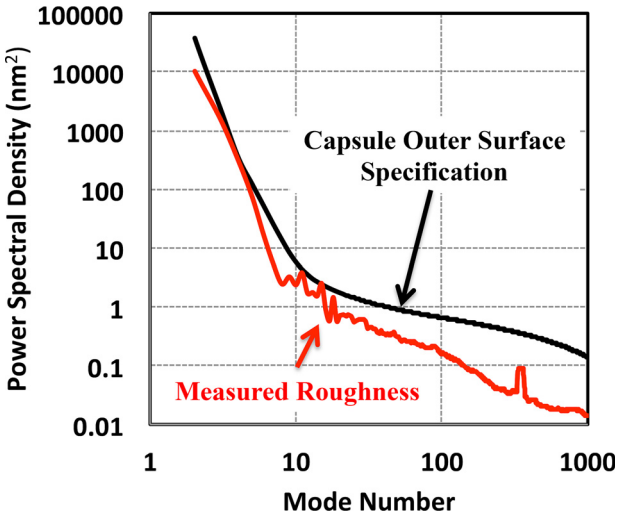


FIG. 4. Power spectra of the measured capsule outer-surface roughness compared to the NIF outer surface specifications for 4-shock AS shot N141123. The modulation power spectrum was obtained by averaging power spectra of multiple Atomic Force Microscope (AFM) measurements taken across the capsule.

The effects of ice surface grooves can be characterized by using a parameter $K$, defined as a sum over all defects with areas $A_i$ and lengths $L_i$ as $K = \sqrt{\frac{1}{V_{fuel}}\sum_{i=1}^{N} A_i^2 L_i}$, where

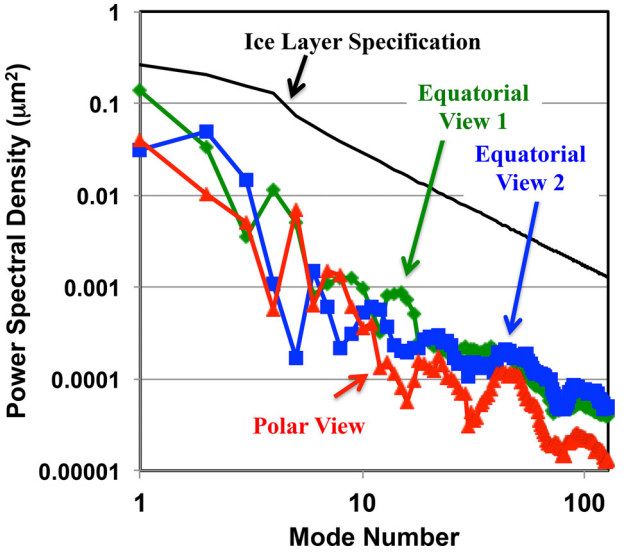


FIG. 5. Power spectra of the inner ice roughness were measured in two equatorial views and one polar view and compared to the NIF inner ice surface specifications for the 4-shock AS shot N141123.

$V_{fuel}$ is the volume of the DT fuel.[7] The specifications[7] have been set requiring K < 0.70 $\mu$m, and the largest groove area $A$ required to be <200 $\mu$m$^2$. For shots N141123 and N150416, both K and A values were close to specifications, while for the shot N150115 both K and A were significantly exceeding the specifications, as shown in Table I. The dust particles on the outer surface were also characterized. The specifications required that no single particle with a volume greater than 30 $\mu$m$^3$ should be present on a capsule surface.[7] This specification was met in the shot N141123. In the shots N150115 and N150416, each had one particle detected with volumes of 35 $\mu$m$^3$ and 50 $\mu$m$^3$, respectively, just outside of the requirements. The specifications for the particle volume were set to minimize the effects of the ablator mix into the DT hot spot near peak compression. All three shots used 30-nm thick membranes (tents) to support capsules in the hohlraums.[7,17] The results of the ablator-mix measurements will be discussed below in Sec. VIII.

## V. NEUTRON PERFORMANCE

Figure 6 shows measured neutron performance results for the layered DT adiabat-shaped shots (N141123, N150115, and N150416) and compares them with all previous LF and HF layered DT implosions, as well as implosions with high-density carbon (HDC) and beryllium (Be) ablators. The measured total neutron yields were plotted as a function of measured down-scattered ratios (DSRs). Fuel compression, or $\rho$R, is related to the DSR of scattered neutrons in the energy range from 10 to 12 MeV, relative to primary neutrons in the range from 13 to 15 MeV.[53] The down-scattered neutrons determining the DSR are mostly scattered in the DT fuel, and in simulations, the DSR is proportional to the fuel areal density: $\rho$R (g/cm$^2$) ~ 19.3 × DSR.[37] In addition, the arrows in Fig. 6 compare the results of the AS shots with their corresponding encircled companion LF and HF shots. The data are also summarized in Table I.

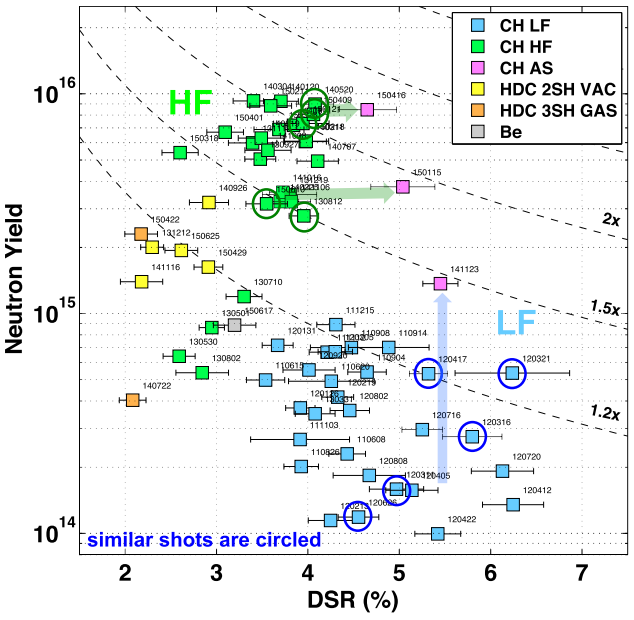


FIG. 6. Measured total DT neutron yield plotted against the ratio of down-scattered 10–12 MeV neutrons over primary 13–15 MeV neutrons (down scattered ratio) for low-foot (LF), high-foot (HF), and adiabat-shaped (AS) drives. Dashed curves represent contours of the calculated yield increase due to alpha heating. Implosions with high-density carbon (HDC) and Beryllium (Be) ablators are also included. The circled data points represent companion shots used to compare with their specific adiabat-shaped shots.

The total neutron yield performance for the 4-shock AS shot N141123 was improved by factors ~3 to ~10, compared to five companion LF shots (driven with similar targets at the same implosion velocity[36]) circled in blue, while measured compression was similar to its LF companions. The level of yield amplification due to alpha heating in this shot, shown by the dashed curve in Fig. 6, was 1.47 ± 0.04. The measured DSR was improved in 3-shock AS shot N150115 by ~25%- to ~36%, compared to its two companion HF shots N130812 and N150610, while the neutron yield was improved by ~20%. For the high-power 3-shock AS shot N150416, the compression was reduced compared to the lower-power 3-shock AS shot. The total neutron yield was $8.46 \times 10^{15} \pm 0.19 \times 10^{15}$, very similar to the companion HF shots N140520 ($8.89 \times 10^{15} \pm 0.18 \times 10^{15}$), N150121 ($7.33 \times 10^{15} \pm 0.19 \times 10^{15}$), and N150409 ($8.06 \times 10^{15} \pm 0.15 \times 10^{15}$), while the calculated level of yield amplification due to alpha heating of 2.42 ± 0.19 was the highest of all shots on NIF. These measurements, along with other results shown in Table I, will be discussed below in Sec. XI.

## VI. HOT SPOT X-RAY IMAGES

Figure 7 shows measured hot-spot x-ray images at peak compression for the three adiabat-shaped shots, captured with photon energies >8 keV.[54] The left-side images in Fig. 7 show equatorial hot-spot shapes, while right-hand-side images show polar shapes. The imploded core emission showed good hot-spot symmetry for all three shots with the asymmetries mostly in modes 2, 3, and 4. The hot-spot distortion specification was <25% rms (Ref. 7) for the deviation from round of the emission contour at 17% of the peak brightness. For the 4-shock AS shot N141123, the measured hot-spot distortion was 14% ± 2% rms, for the 3-shock AS shot N150115 11% ± 1% rms, and for the high-power 3-shock AS shot N150416 also 11% ± 1% rms. The size of the x-ray hot spot was smaller for the 4-shock AS shot and slightly larger in 3-shock AS shots, consistent with lower compression (DSR), measured in 3-shock AS shots. While hot-spot symmetry was generally acceptable, the cold DT fuel asymmetries were very high, as described in Sec. VIII.

## VII. NEUTRON IMAGES AND SHELL COMPRESSION

Figure 8 shows measured primary 14.7-MeV neutron images[55] at peak compression for the three adiabat-shaped shots. As in the case with x-ray images, the measured image size $P_0$ was smaller for the 4-shock AS shot and slightly larger in 3-shock AS shots, consistent with measured compression. In general, the asymmetries were similar or slightly larger for neutron images, compared to x-ray images.

The fuel compression was measured with a magnetic recoil spectrometer (MRS),[53] and four neutron time of flight detectors (NTOFs):[56] SpecA, SpecE, SpecSP, and NITOF. The data from five detectors were used to determine average

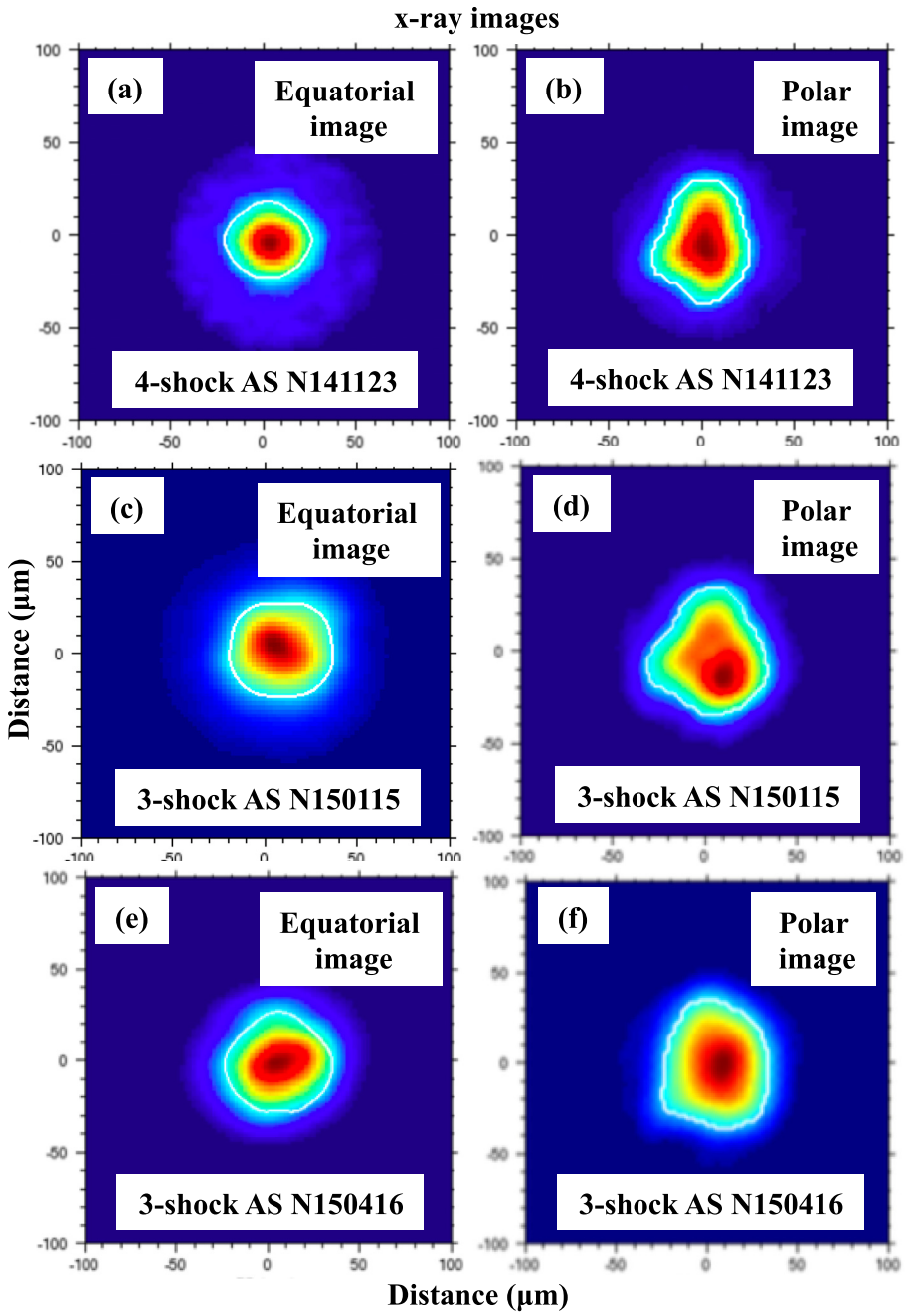


FIG. 7. Measured time-integrated, hot spot x-ray images in equatorial (a), (c), and (e) and polar views (b), (d), and (f) for three AS experiments N141123, N150115, and N150416.

DSRs. The locations of these five detectors on the NIF target chamber are shown in Fig. 9(a). Each detector probes a certain part of the fuel, approximately shown in Fig. 9(b) using Monte-Carlo calculations assuming a point source of primary 14.7-MeV neutrons probing a spherical shell. In experiments, the DSR detectors cover a somewhat larger surface area, than shown in Fig. 9(b), with a solid angle of $\sim 1\ \pi$ due to a finite size of the primary neutron source. It is important to point out that not all the volume of the DT fuel is probed while more than one detector probe some fuel areas. This can lead to some degree of sampling bias when comparing the inferred average compressions on different shots using these DSR detectors.

Figure 10 shows measured DSRs for these five detectors as a function of polar angle of the NIF target chamber. On average, three nearby detectors MRS, NITOF, and SpecA, located around azimuthal angle $\varphi \sim 315°$, consistently show slightly higher compression than SpecE, located at $\varphi \sim 174°$. This observation is consistent with low-mode asymmetry, also detected in a number of HF shots. The measured average DSRs were 5.45% ± 0.19%, 5.04% ± 0.35%, and 4.65% ± 0.23%, for shots N141123, N150115, and N150416, respectively.

While DSR measurements were primarily sensitive to the DT fuel $\rho$R, the x-ray emission at peak compression was used to estimate plastic shell $\rho$R around peak compression. The shell optical-depth (OD) attenuation at 10.9 keV, shown in Table I, was calculated using time-integrated x-ray hot-spot images measured with differentially filtered pinholes ("Ross pairs").[54] The OD attenuation had a small

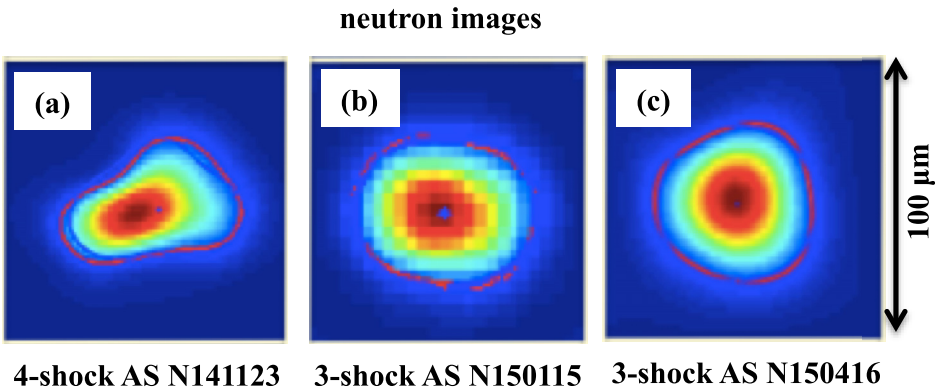


FIG. 8. Measured hot spot, neutron images in equatorial view in three AS experiments (a) N141123, (b) N150115, and (c) N150416.

contribution from the compressed DT shell of about ~0.2 OD, but primarily depended on attenuation of the cold plastic ablator. The compressed plastic ablator $\rho$Rs were estimated using the cold opacity of the plastic shell at 10.3 keV, including Si-doped layers, (see Table I). The shell opacity can be reduced, compared to cold values, by a small amount of ~10%–20% due to its heating near peak compression. Total $\rho$Rs of the DT fuel and compressed plastic shell were estimated to be $1.63 \pm 0.20$ g/cm$^2$, $1.33 \pm 0.12$ g/cm$^2$, and $1.11 \pm 0.10$ g/cm$^2$, for shots N141123, N150115, and N150416, respectively.

Fuel compression has also been inferred using measurements of Au isotope ratios with a solid radiochemistry (SCR) diagnostic.[57] Neutrons interact with Au atoms present in the hohlraums and can produce $^{196g}$Au and $^{198t}$Au isotopes. Down-scattered neutrons contribute to the production of the $^{198t}$Au with (n, $\gamma$) reaction, while they do not significantly contribute to the production of $^{196g}$Au, the (n, 2n) reaction, which has a threshold. As shown in Ref. 58, the ratio $^{198t}$Au/$^{196g}$Au is related to the DSR. Figure 11 shows measured $^{198t}$Au/$^{196g}$Au ratios as a function for measured DSR for low-foot, high-foot, and adiabat-shaped experiments. The uncertainties for measured $^{198t}$Au/$^{196g}$Au ratios are much smaller than for DSR measurements in adiabat-shaped experiments. These measurements confirmed that fuel compression with 4-shock AS drive was similar to the highest

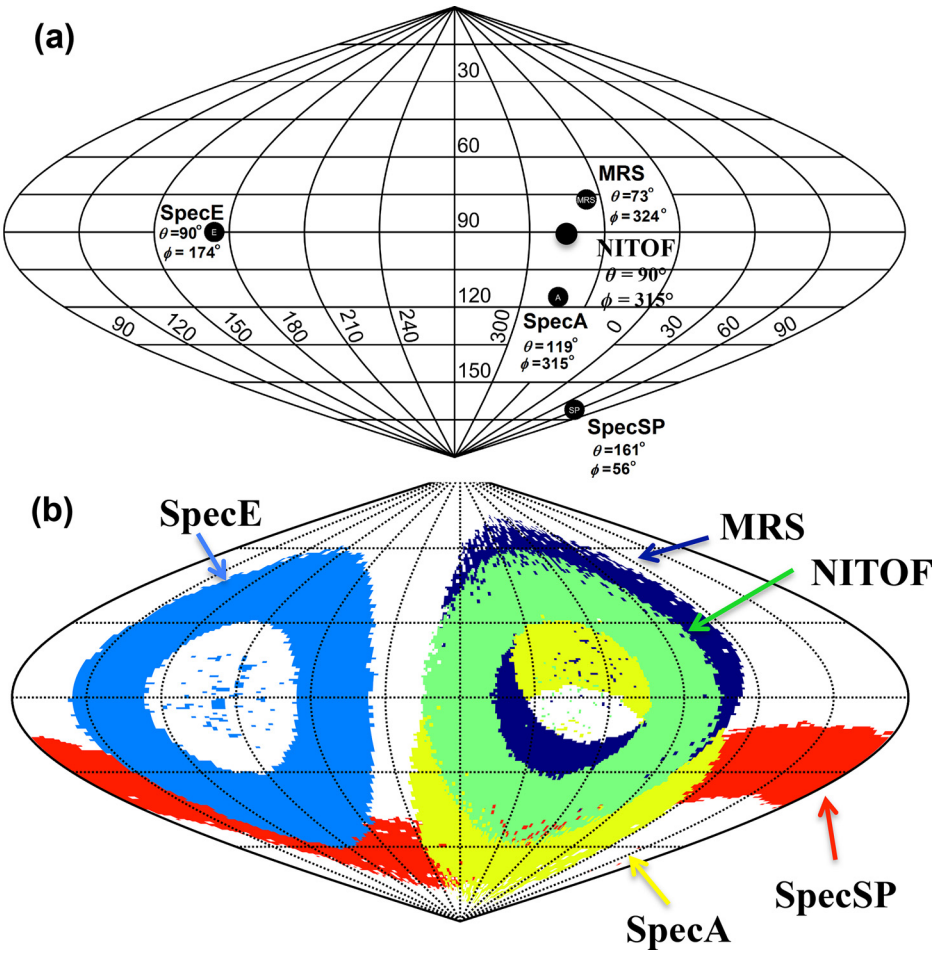


FIG. 9. (a) Locations of the five DSR detectors on the NIF target chamber. (b) Each detector probes a certain part of the fuel shown as distributions of down-scattered neutrons on a sphere using Monte-Carlo calculations assuming a point source of primary 14.7-MeV neutrons probing a spherical DT shell.

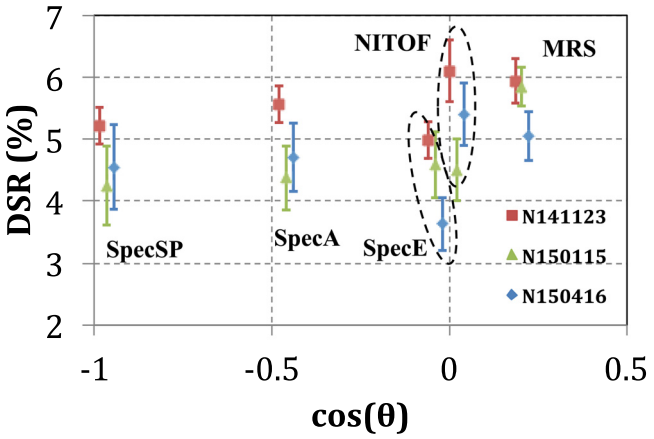


FIG. 10. Measured DSR values for five DSR detectors as a function of the cosine polar angle of the NIF target chamber for three AS experiments.

compression achieved in LF experiments and, for the shot N150416, it was similar to the highest compression achieved in the HF shots. The measured compression for the 3-shock AS shot N150115 was higher than in all HF experiments. This will be further discussed in Sec. XI.

## VIII. LOW-MODE ρR MODULATIONS OF COMPRESSED FUEL

The low-mode asymmetries with mode numbers <10 were measured using Flange Neutron Activation Diagnostic (FNAD) detectors.[59] Figure 12 shows maps of the FNAD results for the three adiabat-shaped shots, as well as locations of the FNAD detectors on the NIF target chamber in addition to locations of MRS and NTOFs, shown in Fig. 9(a). The maps show measured ratios of the primary 14.7 MeV neutron yields over the average neutron yield, $Y/Y_{ave}$, for seventeen FNAD detectors, used in each of these experiments. In addition, the color maps show low-mode fits to the FNAD data. For each FNAD detector, the ratio $Y/Y_{ave}$ is a measure of the unscattered primary neutrons remaining in the direction to

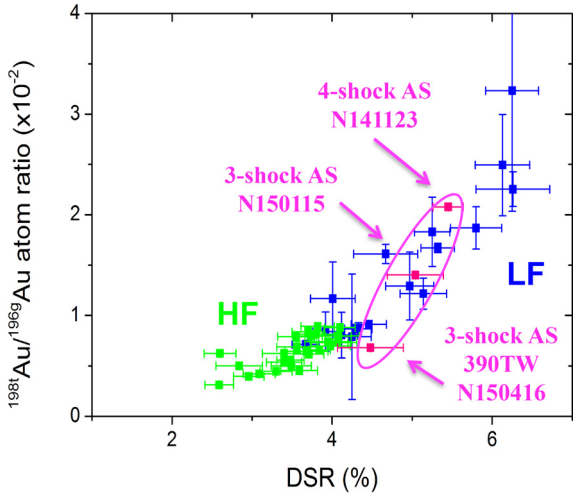


FIG. 11. Fuel compression measured with $^{198t}$Au/$^{196g}$Au isotope ratios from solid radiochemistry (SCR) collectors as a function of measured DSR for HF, LF, and three AS shots. Low uncertainties in Au isotope ratios allow us to clearly distinguish compressions in AS shots, while their DSR measurements show larger uncertainties.

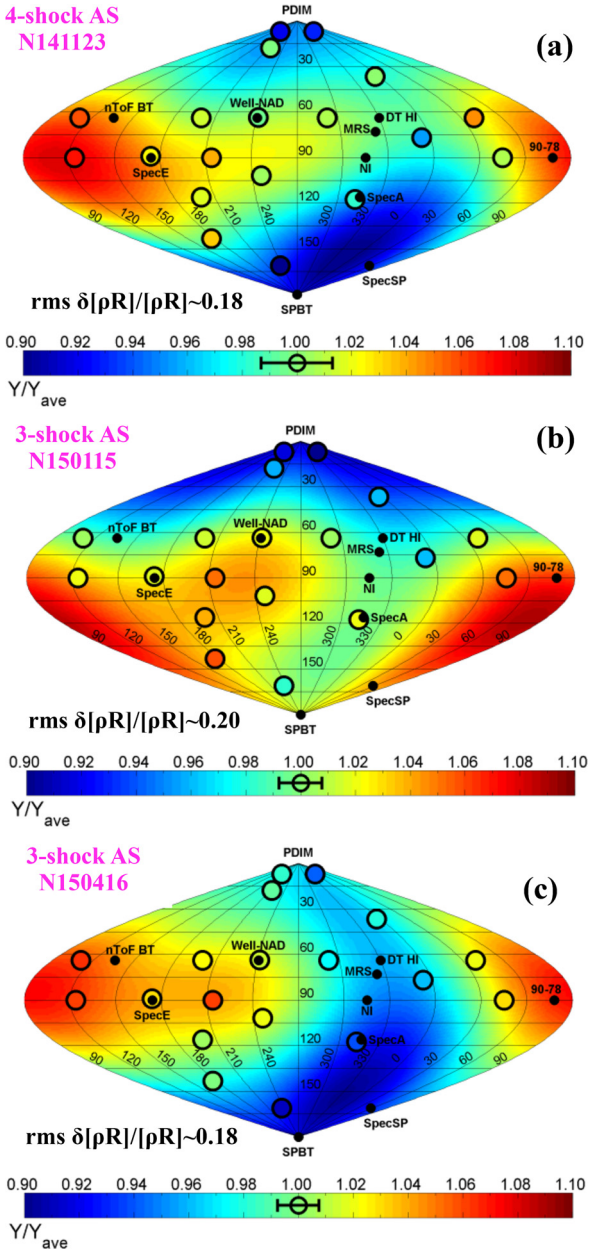


FIG. 12. Maps of neutron yield ratios over average neutron yield $Y/Y_{ave}$, for seventeen Flange Neutron Activation Diagnostic (FNAD) detectors for three AS shots (a) N141123, (b) N150115, and (c) N150416. Also shown the locations of FNAD detectors on the NIF target chamber along with five DSR detectors. The color represents low-mode fits to the data.

this particular detector. It also depends weakly on the bulk velocity of the hot-spot toward to (or away from) this detector. After the effect of the bulk velocity is removed, the FNAD data can be used to infer low-mode asymmetries of the compressed DT shell at peak compression.

Figure 13 shows the measured low-mode ρR asymmetries with rms shell integrity of $\delta(\rho R)/\rho R$ as a function of fuel compression ρR for LF, HF, and three adiabat-shaped implosions. In Fig. 13(a), the results from 4-shock (N141123) and 3-shock (N150115) AS shots that are circled in red are compared with their corresponding LF and HF shots, circled in blue and green, respectively. The results from high-power 3-shock AS shot N150416 are compared with its three

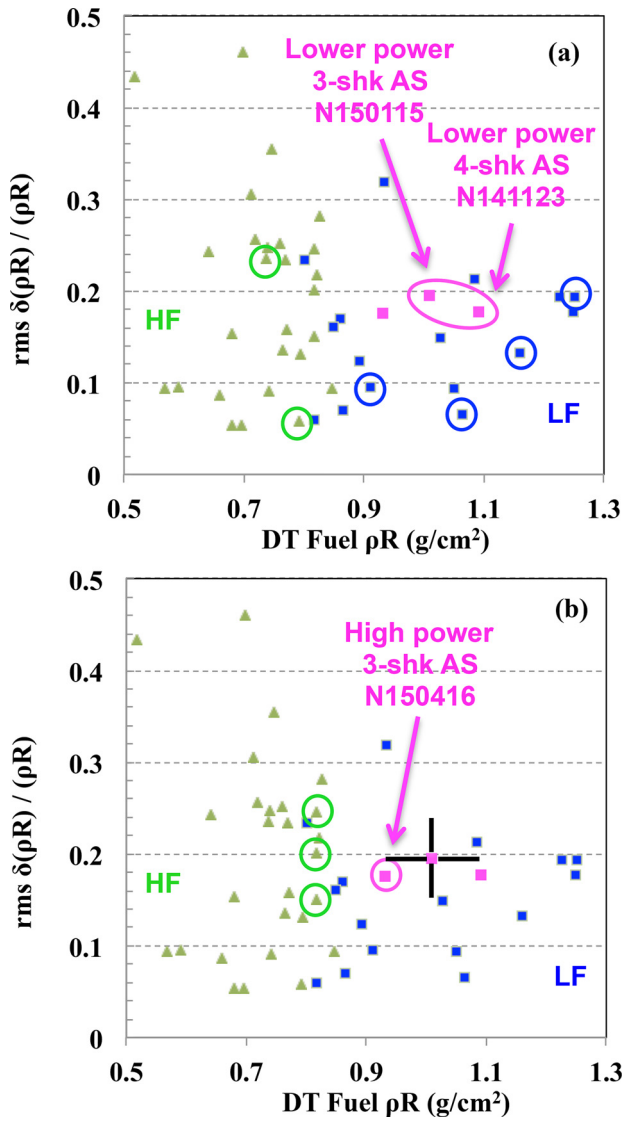


FIG. 13. (a) Measured low-mode $\rho$R asymmetries with rms shell integrity of $\delta(\rho R)/\rho R$ as a function of fuel compression $\rho$R for LF, HF, and three AS implosions. The results from 4-shock (N141123) and 3-shock (N150115) AS shots are circled and compared with their corresponding low-foot and high-foot shots, also circled. (b) The same figure as (a) but with results from 3-shock high-power AS shot N150416 circled and compared with its corresponding three high-power HF shots. Representative uncertainties are shown for the shot N150115.

corresponding HF shots in Fig. 13(b). All three adiabat-shaped shots had significant measured low-mode asymmetries, with rms $\delta(\rho R)/\rho R$ of ~0.2. The 4-shock AS shot N141123 had asymmetries either higher or similar than in its companion LF shots while the neutron yield was ~3 to ~10 times higher than in these LF shots. This indicates that low-mode asymmetries were not the dominant source of degradation in LF shots, compared to high-mode modulations that were significantly reduced with adiabat shaping. For the 3-shock AS shot N150115, the low-mode asymmetries were similar to the companion HF shots while the compression was significantly increased compared to the HF shots.

The low-mode fits to FNAD data show thick fuel areal-density areas in polar regions, a pattern that is repeatable in the three adiabat-shaped shots, and in general also in the HF and LF shots. Such asymmetries can be created due to low-mode drive asymmetries and as well as high-mode modulations such as tents and fill tubes. However, better understanding of the origin of these modulations is needed before they can be mitigated.

## IX. ABLATOR MIX INTO HOT SPOT

Figure 14 shows the measured neutron yield as a function of the x-ray enhancement ratio that is the measure of the plastic ablator mix into the DT hot spot. The x-ray enhancement ratio was defined using a ratio of the measured hard x-ray yield to the neutron yield.[18] It is a measure of the ablator mix due to its dependence on hot-spot effective Z, as described in Ref. 18. Experiments with the x-ray enhancement ratio near ~1 indicate an absence of ablator mix, while the shots with a high enhancement ratio indicate a high ablator mix. All three adiabat-shaped shots show low levels of the ablator mix, as all HF shots. Five circled companion LF shots to the 4-shock AS shot show various amounts of ablator mix, correlated with a degradation of neutron yield. It is interesting to notice that two of these companion LF shots had small amounts of mix, as in the 4-shock AS shot, but the yield performance was ~3× lower than in the 4-shock AS shot. These observations will be further discussed in Sec. XI.

## X. HOT-ELECTRON MEASUREMENTS

Time-integrated, hard x-ray emission images (with photon energies >50 keV), associated with hot-electrons, were measured by the equatorial hard x-ray imager (EHXI)[60] and presented in Figs. 15, 16, and 17, for the shots N141123, N150115, and N150416, respectively. These images and corresponding vertical lineouts were compared with their companion LF and HF shots, as indicated in the figures. The images and lineouts indicate locations of the emission from

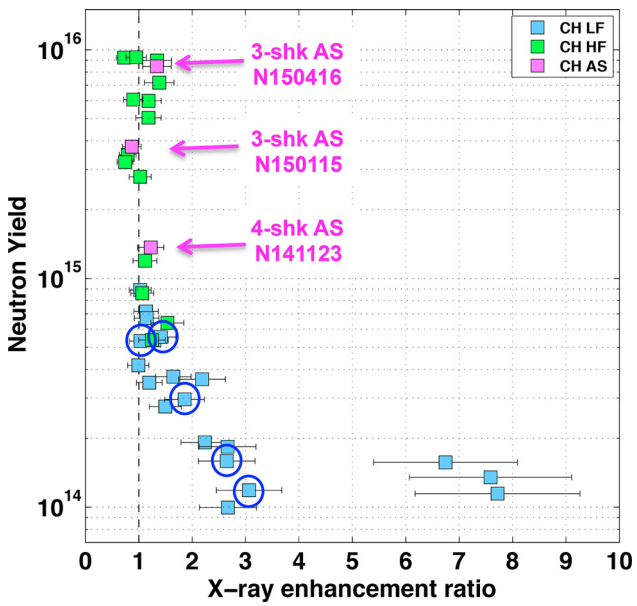


FIG. 14. Measured neutron yield as a function of x-ray enhancement ratio (which is the measure of the ablator mix into the DT hot spot) for LF, HF, and three AS experiments. Circled are five companion low-foot shots to the 4-shock AS shot N141123.

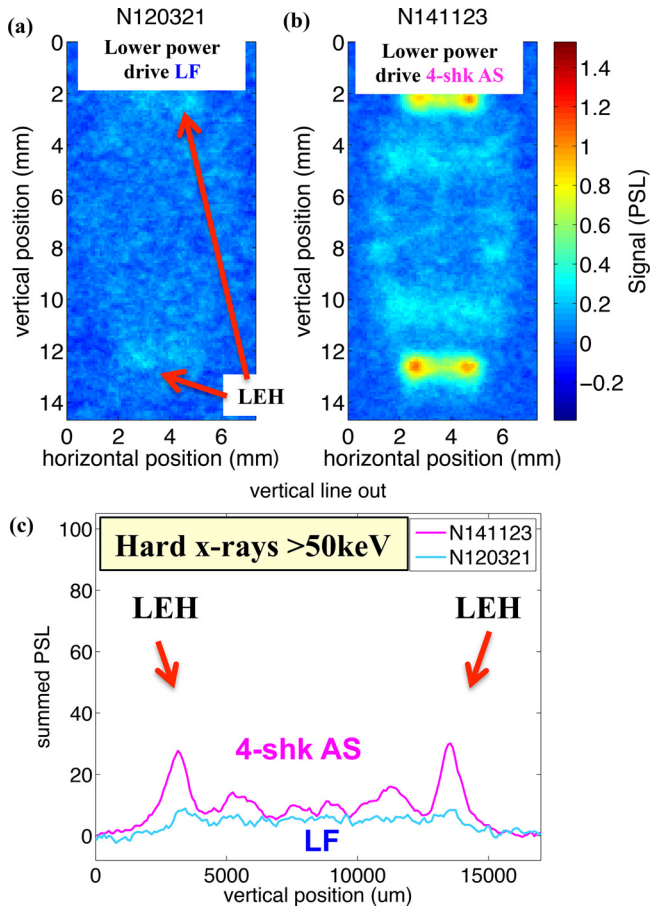


FIG. 15. Hard x-ray (>50 keV) images from the hohlraums for (a) LF shot N120321 and (b) companion 4-shock AS shot N141123 measured with EHXI diagnostic. (c) Vertical lineouts of the emission for each shot showing similar x-ray signals in the central parts of the hohlraums, away from the laser entrance holes (LEHs). The central parts of the lineouts were corrected for slightly different filtration used in N120321, but emission from LEH could not be properly corrected.

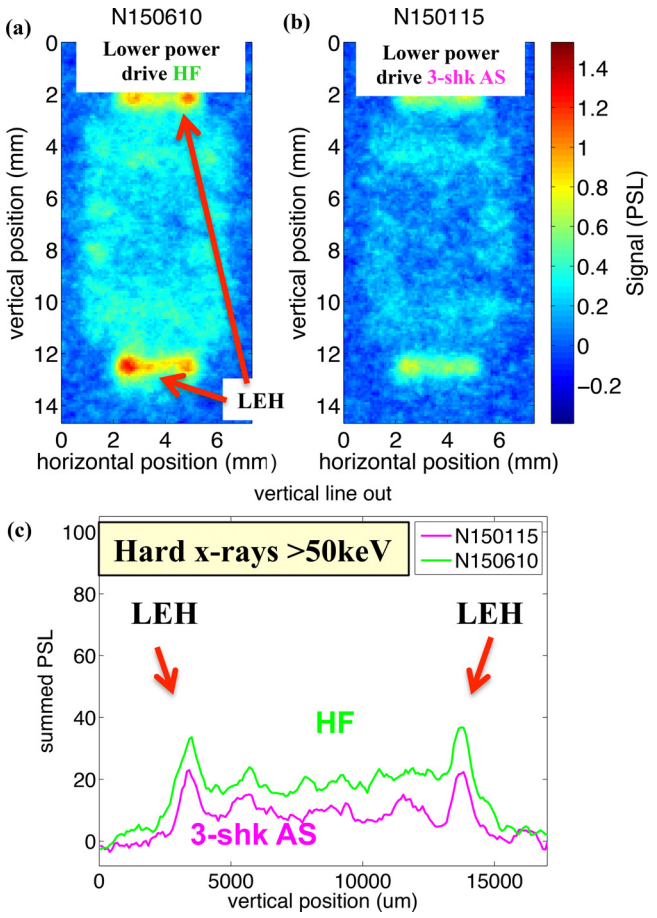


FIG. 16. Hard x-ray (>50 keV) images from the hohlraums for (a) HF shot N150610 and (b) companion 3-shock AS shot N150115 measured with EHXI diagnostic. (c) Vertical lineouts of the emission for each shot.

laser entrance holes (LEHs) and from the central parts of the hohlraums. While the emission is similar in the low power 4-shock and 3-shock AS shots (see the lineouts in Figs. 15 and 16), it is nearly doubled in the high-power 3-shock AS shot (compare with the lineout in Fig. 17). This increase can be responsible to the fuel preheat and some reduction of the fuel compression for the 3-shock AS shot N150416.

The electron preheat can come from electrons generated by the Stimulated Raman Scattering (SRS) and Two-Plasmon Decay (TPD) instability.[38] In current experiments, the electron temperatures attributed to SRS are ~18 keV, while the component attributed to TPD is much higher, ~100 keV. It is interesting to notice that the hot-electron signals were generally lower in adiabat-shaped shots than in companion HF shots. Therefore, hot electrons might also contribute to overall lower compression in HF experiments. Time dependence of hot electrons has a crucial effect on fuel preheat. Hot-electron preheat can be more detrimental if it happens before the arrival of the first shock in the DT fuel. While time-resolved hard x-ray signals were not possible to measure in layered DT implosions due to high neutron backgrounds, they were measured in tuning shots at similar conditions to that in DT implosions. It was estimated that the fuel preheat before the break-out of the first shock into the hot spot is about three orders of magnitude higher in low-power 3-shock AS shot N150115, compared to the 4-shock AS shot N141123, while it is slightly lower (a factor of ~2) in companion low-power HF shots.[61] The electron preheat was previously studied in simulations and discussed in Ref. 38.

## XI. DISCUSSION

One of the most important questions in ICF is the role of hydrodynamic instabilities in degradation of implosion performance and quantitative understanding of deviations from 1-D predictions. More specifically, what are the relative contributions of low-mode modulations including drive asymmetries and high-mode modulations on performance degradation as a function of fuel compression (convergence) and implosion velocity? As it has been shown in layered implosions on OMEGA,[60] the experimental yield $Y_{exp}$ can be expressed as $Y_{exp} \sim V_{imp}{}^{5}\,\alpha$, while the 1-D yield is scaled as $Y_{1\text{-}D} \sim V_{imp}{}^{6}\,\alpha^{-0.8}$, where $V_{imp}$ is the implosion velocity and $\alpha$ in the DT fuel adiabat. In the 1-D scaling, lower adiabat $\alpha$ (and as a result higher compression of the DT fuel) increases the neutron yield. However, the experimental yield is proportional to adiabat $\alpha$, indicating that the detrimental effects of hydrodynamic instabilities on the neutron yield increase at higher compression in OMEGA implosions.[62]

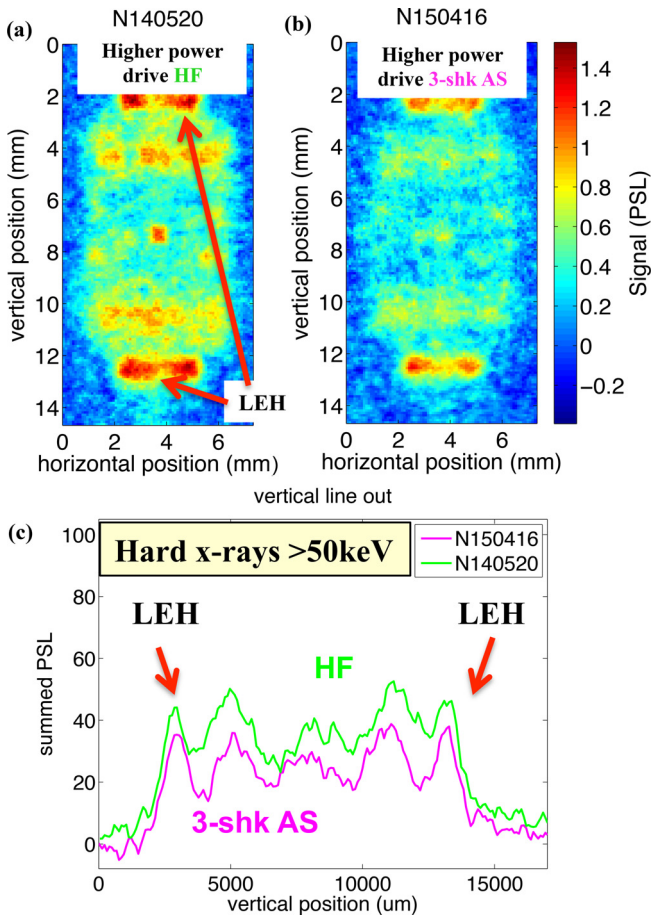


FIG. 17. Hard x-ray (>50 keV) images from the hohlraums for (a) high-power HF shot N140520 and (b) companion high-power 3-shock AS shot N150416 measured with EHXI diagnostic. (c) Vertical lineouts of the emission for each shot.

Before the adiabat-shaping campaign, such a trend was also observed in the 2× larger-scale indirectly driven capsules on NIF. As it can be seen in Fig. 6, generally higher yields were measured at lower compression in HF implosions, while generally lower yields were measured at higher compression in LF implosions. However, the LF implosions were much more unstable than HF implosion at the ablation front, as shown in Fig. 1(b), resulting in ambiguity over effects compression vs instability on yield. The 3-shock adiabat-shaped implosion N150115 isolated the compression effect on implosion performance, as the ablation front stability was similar to that in HF. The DT fuel compression was significantly increased up to ∼36%, compared to its companion HF implosions driven at the same implosion velocities of ∼330–340 km/s. Such an increase in compression was achieved despite very significant low-mode asymmetries in DT fuel with rms $\delta(\rho R)/\rho R$ of ∼0.2. This indicates that low-mode asymmetries might not be the dominant factor for the reduced compression in the companion HF shots at similar levels of low-mode asymmetries as in shot N150115 [see Fig. 13(a)]. While the compression increased, the neutron yield also increased by ∼20%, reversing the trend observed on OMEGA.[62] However, the ∼20% increase is lower than ∼50% increase expected from 1-D scaling for which $Y \sim (\rho R)^{1.5}$,[63] suggesting that the hydrodynamic instabilities affect the performance at these conditions. It is noteworthy that the increases in the compression and the yield were despite high roughness of the DT ice layer, well above the specifications and also versus companion HF shots (as discussed in Sec. IV). This indicates that large ice roughness might not be an important factor for the degradation of the fuel compression at present conditions.

The measured increase in compression up to ∼36% was actually larger than the ∼10% increase that was expected to result from the ∼10% lower adiabat in the AS design relative to the HF shots with lowest simulated adiabats (the simulated adiabats in HF shots varied from ∼2.2 to ∼2.7). As a possible explanation for this unexpectedly large increase in compression, we note that measurements of the hot-electrons were significantly reduced with the AS drive, compared to the HF drive.[37,38] The number of hot electrons with energy >170 keV is reduced by a factor of ∼10 as measured in shape-tuning experiments with plastic capsules with similar drives to the layered DT implosions.[37] (Hot electrons cannot be reliably measured in the high-yield DT layered implosions.) In complementary EHXI measurements shown in Fig. 16, the number of hot electrons with energy >50 keV was also reduced by a factor of ∼2. These observations suggested a hypothesis that the hot-electron preheat could compromise compression, especially in the HF implosions, where the hot-electron signals were even higher.

This hypothesis was supported by the results of the high-power, 3-shock AS shot N150416. When the peak power was increased from 330 TW to 390 TW, the neutron yield was increased more than 2× compared to the lower-power AS shot N150115. However, the DT fuel $\rho R$ from DSR measurements was reduced, in agreement with the reduction in compression inferred from Au isotope ratios, as shown in Fig. 11. This compression reduction was correlated with increased hot-electron signals, shown in Figs. 16 and 17. The compression was reduced to DSRs ∼4.65% ± 0.32%, almost to the same levels as measured in the companion high-power HF shots with DSRs ∼4%, shown in Fig. 6. The companion HF shots had even higher hot-electron signals than the AS shot (see the comparison in Fig. 17). Another hypothesis for the measured compression in high-power HF shots, apart from the preheat hypothesis, is due to low-mode asymmetries, based on 2-D and 3-D simulations.[64] In these simulations, the compression was degraded from 1-D levels with DSRs of ∼6.5% to the near measured levels with DSR ∼4% primarily due to time-dependent low-mode asymmetries[64] in high-power HF shots. Therefore, some combination of preheats and low-mode asymmetries are possible for compression reduction in the high-power HF shots. It is interesting to notice that while low-mode asymmetries varied almost by a factor of ∼2, the neutron yield was very reproducible (within ∼10%) in these three companion high-power HF shots [see Fig. 13(b)]. This result indicates that variations of low-mode asymmetries by a factor of ∼2 were not enough to affect HF implosions with DSR ∼ 4%. Proposed experiments with improved and/or degraded low-mode asymmetries are expected to provide more quantitative insights of their importance in layered implosions.[64] Both high-power HF drive and

especially 4-shock AS drive (due to its higher sensitivity at higher compression) are important platforms for such studies.

In the experiment with the 4-shock adiabat-shaped drive, the neutron yield was improved by factors ~3 to ~10, compared to five companion LF shots, while measured compression was similar to its LF companions (see Fig. 6). The neutron yield increased despite larger low-mode asymmetries of DT fuel with rms $\delta(\rho R)/\rho R$ of ~0.2 than in two companion LF shots. It is interesting to notice high yield variability (with a factor of ~4) of the five companion LF shots, shown in Fig. 6. The yield reduction in these LF shots was correlated with an increased ablator mix into the DT hot spot, shown in Fig. 14, but was not correlated with low-mode asymmetries, as shown in Fig. 13(a). In fact, one of the better performing LF shots N120321 (with highest yield and DSR) out of five companions had the largest measured low-mode asymmetries. These observations suggest that the dominant degradation source for LF implosions was seeded by ablation-front instability growth, since adiabat shaping and smaller tents (30-nm vs 110-nm) significantly stabilized this growth, compared to LF experiments [see Fig. 1(b)]. Two of the companion LF shots (N120321 ands N120417) show negligible amount of the ablator mix as in 4-shock AS shot N141123, yet their yield performance was ~3 times lower than in the AS shot (see Fig. 14). This suggests that the feed-through of modulations from ablation front to the hot spot boundary had a significant effect on the DT burn in these two LF shots. This is a very important result indicating that significant degradation due to high-mode instability growth can occur due to cold fuel and hot-spot mix, without the ablator mix into the hot spot.

One of the goals of the adiabat shaping campaign was the study of the effects of high-mode instability growth on implosion performance. The instability growth was modified by adiabat shaping and tent thickness simultaneously in this campaign. Therefore, the reduction in instability growth and subsequent neutron yield improvement in the 4-shock AS shot N141123 could come not only from adiabat shaping but also from thinner, 30-nm thick tents instead of 110-nm thick tents used in LF companion shots. Using thinner tents in LF implosions did not result in performance improvements. One of the LF shots (LF130331) used 15-nm thick tent, compared to the nominal 110-nm thickness used in the majority of the LF shots. The capsule was driven at an implosion velocity of ~305 km/s and had measured DSR of ~4.1% in this shot. The measured neutron yield was $\sim 3 \times 10^{14}$ in this shot, similar to other LF shots with thicker tents driven at comparable implosion velocities and DSRs. The adiabat shaping reduced not only instability growth factors[35] but also the growth of tent modulations,[33] as was shown in radiography experiments by comparing to a companion LF shot with the same tent thickness.[33] These observations suggested that the adiabat shaping was the dominant contributor to the performance improvements over LF implosions, not the tent thickness by itself. Varying the tent thickness in companion adiabat shaped and LF implosions will provide more stringent tests of the relative effects of the tent thickness vs adiabat shaping on implosion performance.

The neutron yield in the 4-shock AS shot N141123 was about 2.7 times lower than in the 3-shock AS shot N150115, driven at a similar velocity of ~320–330 km/s. It was proposed to improve ablation-front stability with 4-shock AS drive to the levels of the 3-shock AS and HF drives. This has been already achieved in simulations by increasing the energy in the first picket from 22 kJ to 30 kJ.[38] Such an experiment will provide a further scaling of neutron yield as a function of compression at the same low level of ablation-front stability as the 3-shock AS shot N150115 but with the higher compression (DSR of ~5.5%) attainable with a 4-shock AS drive.

Prior to the DT implosion, the backlit x-ray radiographs of imploding capsules driven by the 4-shock AS drive, showed a large $P_4$ mode.[33] It was expected to significantly reduce neutron performance per 2-D and 3-D simulations.[64] To test the importance of low-mode asymmetries on neutron yields and DSRs, capsule "shimming" was proposed[65,66] by varying pre-imposed $P_2$ and $P_4$ modes. The 4-shock AS drive had higher compression, compared to HF drives, so it is more favorable platform for such a study due to higher sensitivity at higher convergence.

In addition to the neutron yield and DSR, the performance can also be characterized by other important ICF parameters, inferred from experimental data. They include hot-spot pressure P, a parameter $P\cdot\tau$, which is the product of hot-spot pressure and confinement time $\tau$, the ignition threshold factor parameter IFTX, the Generalized Lawson Criterion (GLC), and yield amplification due to alpha heating.[67–70] They are summarized in Table I for the three AS shots. The product time $P\cdot\tau$ depends on two major ICF parameters,[59] total shell areal density at peak compression $\rho R$ and implosion velocity V as, $P\cdot\tau(\text{Gbar ns}) = 85(\rho R)_{total}\frac{V(\text{cm/s})}{10^8}$. The GLC is defined as a ratio of $P\cdot\tau$ to ignition $(P\cdot\tau)_{IGN}$. It depends on the product of the hot-spot pressure (inferred from simple models based on experimental observables), confinement time $\tau$, as well as the ion temperature T. The ITFX depends on two measured quantities: the DT neutron yield in the range from 13 to 15 MeV, $Y^{DT}_{13-15\,\text{MeV}}$, and the DSR as, $ITFX = \left(\frac{Y^{DT}_{13-15\,\text{MeV}}}{4.0e^{15}}\right)\left(\frac{DSR}{0.067}\right)^{2.1}$.[67–69] The yield depends on the hot-spot performance and the DSR is the measure of the fuel compression $\rho R$, which determines the confinement time. The GLC and ITFX are equivalent, $GLC \approx (ITFX)^{0.375}$, and serve complementary purposes.[67–69] GLC can be calculated from ITFX and independently from $P\cdot\tau$, as shown in Table I. Generally, the GLC is the more uncertain performance metric due to its model dependence; while ITFX is defined directly from the measured quantities $Y^{DT}_{13-15\,\text{MeV}}$ and DSR.

Yield amplification due to alpha heating is another important performance metric. It is defined using parameter ITFX calculated with and without alpha heating,[67,68] as shown in Fig. 18. Ignition has been defined as $ITFX_{no\,\alpha}$ ~1.0, corresponding to the yield amplification ~100, as shown in Fig. 18. The total neutron yield in the high-power 3-shock adiabat-shaped shot N150416 was $8.5 \times 10^{15} \pm 0.2 \times 10^{15}$, with an average fuel areal density of 0.90 $\pm$ 0.07 g/cm$^2$, corresponding to the ignition threshold factor parameter IFTX (calculated without alpha heating) of

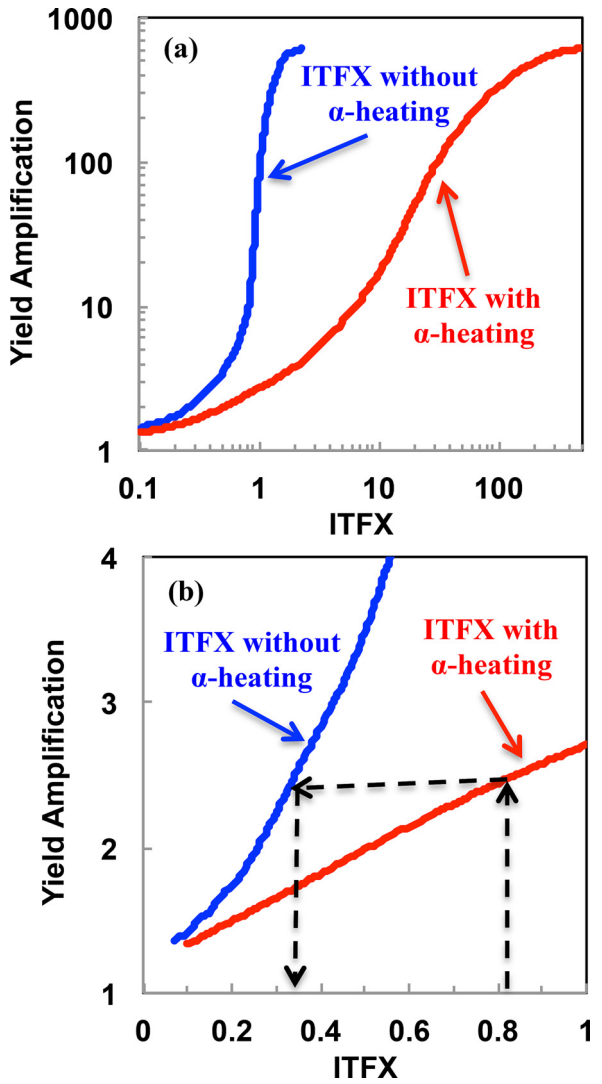


FIG. 18. (a) Yield amplification due to alpha heating as a function of ITFX calculated with and without alpha heating. (b) The same figure zoomed at lower alpha heating range with values of ITFX and yield amplification indicated for high-power, 3-shock AS shot N150416 as dashed lines.

$0.34 \pm 0.03$.The performance parameter IFTX and corresponding yield amplification were among the highest of all shots on NIF and the closest to ignition at this time, as also shown in Fig. 6. However, the highest total neutron yield of $9.3 \times 10^{15} \pm 0.2 \times 10^{15}$ was achieved in HF shot N140304, but at lower DT fuel density of $0.66 \pm 0.04$ g/cm$^2$ and lower ITFX (without alpha heating) of $0.25 \pm 0.02$.[23] It is also noteworthy that all three adiabat-shaped shots had the highest measured neutron yields and performance parameters such as ITFXs and yield amplifications, compared to experiments with the same measured compressions (DSRs), shown in Fig. 6.

## XII. FUTURE EXPERIMENTS

One of the important goals of the "adiabat-shaping" campaign was testing the effect of compression on neutron performance. The 3-shock adiabat-shaped implosion N150115 did this by comparing its performance to companion HF shots with similar implosion velocity and the ablation front stability. While the DT fuel compression was increased up to ~36%, compared to its companion HF implosions, the neutron yield also increased by ~10%. This reversed the trend observed on OMEGA.[62] Will this trend hold at higher convergence? Unlike in OMEGA implosions, the alpha heating has significant contribution to neutron yield amplification in adiabat-shaped implosions on NIF; therefore, it could offset the performance degradation due to hydrodynamic instabilities and asymmetries expected at higher convergence. To answer this question, it was proposed to improve ablation-front stability with the 4-shock AS drive to the levels of the 3-shock AS and HF drives.[38] The goal is to achieve the implosion with the DSR of ~5.5% to ~6%, implosion velocity of ~320–330 km/s, at the same ablation-front stability as HF and 3-shock AS drives to compare its performance with the companion HF and AS drives. This new drive has been designed by modifying 4-shock AS drive (used in the shot N141123) by increasing the energy in the first picket from 22 kJ to 30 kJ.[38] In the simulations, the neutron yield is expected to approximately double by such a slight increase in the first picket energy. Further, imposing a modulation with $P_4$ amplitude of $-3.5$ $\mu$m at the outer capsule surface ("shimming") is expected to mitigate the large low-mode $P_4$ asymmetry measured in the tuning shots prior to shot N141123 and increase the total neutron yield to $\sim 1.4 \times 10^{16}$ at DSR~6.3%. Additional $P_2$ shims, increased power and energy (420TW and 1.8 MJ) are predicted to increase the total neutron yield to $\sim 4 \times 10^{18}$ in 2-D simulations.[65] Such experiments will not only provide a further scaling test of neutron yield as a function of compression but also will test predictive capabilities of the simulations at ignition conditions.

One of the important remaining questions for the adiabat-shaping campaign is the reproducibility of the results; therefore, additional repeat experiments are necessary to address it. The performance uncertainties of the companion HF results could be used as a rough guide for the uncertainties in the 3-shock AS implosions since the compression and the implosion velocities were not too distant between these HF and AS experiments. Therefore, neutron yield variability of ~10%–20% rms and the DSR variability of ~10% rms could be used as rough estimates of uncertainties for 3-shock AS experiments. It is more difficult to predict variability of the 4-shock AS implosion, because of the high variability of the companion LF shots, therefore reproducibility shots are more important for the 4-shock AS experiments.

## XIII. SUMMARY AND CONCLUSIONS

In conclusion, layered DT implosions were carried out using 3-shock and 4-shock adiabat-shaped drives and plastic ablators on NIF. The purpose of these shots was to gain understanding of performance degradation in the low-foot implosions during National Ignition Campaign (NIC) and subsequent high-foot implosions. The neutron yield performance in the experiment with the 4-shock adiabat-shaped drive was improved by factors from ~3 to ~10, compared to five companion low-foot shots, while measured compression was similar to its low-foot companions. This indicated that a

dominant degradation source for low-foot implosions was ablation-front instability growth since adiabat shaping significantly stabilized this growth and seeds associated with it. For the experiment with the low-power 3-shock adiabat-shaped drive, the DT fuel compression was significantly increased by between 25% and 36% compared to its companion high-foot experiments. While compression increased, the neutron yield also slightly increased by ~20%. For the experiment with the high-power 3-shock adiabat-shed drive, the DT fuel compression was slightly increased by ~14% compared to its companion high-foot experiments. However, the compression was reduced compared to the lower-power 3-shock adiabat-shaped drive, correlated with the increase of hot electrons that hypothetically can be responsible for reduced compression in high-power adiabat-shaped experiments as well as high-foot experiments. The total neutron yield in the high-power 3-shock adiabat-shaped shot N150416 was $8.46 \times 10^{15} \pm 0.19 \times 10^{15}$, with the fuel areal density of $0.90 \pm 0.07$ g/cm$^2$. The inferred yield amplification was the highest of all shots on NIF so far. Follow-up experiments were proposed to continue testing physics hypotheses, to measure implosion reproducibility, and to improve quantitative understanding on present implosion results.

## ACKNOWLEDGMENTS

The authors would like to thank K. Anderson, R. Betti, V. N. Goncharov, J. D. Lindl, and D. Shvarts for useful discussions. This work was performed under the auspices of the U.S. Department of Energy by Lawrence Livermore National Laboratory under Contract No. DE-AC52-07NA27344 and by General Atomics under Contract No. DE-NA0001808.

[1]J. Nuckolls, L. Wood, A. Thiessen, and G. Zimmerman, Nature **239**, 139 (1972).
[2]S. Atzeni and J. Meyer-ter-Vehn, *The Physics of Inertial Fusion: Beam Plasma Interaction, Hydrodynamics, Hot Dense Matter*, International Series of Monographs on Physics (Clarendon Press, Oxford, 2004).
[3]J. D. Lindl, *Inertial Confinement Fusion: The Quest for Ignition and Energy Gain Using Indirect Drive* (Springer-Verlag, New York, 1998).
[4]E. M. Campbell, R. Cauble, and B. A. Remington, AIP Conf. Proc. **429**, 3 (1998).
[5]V. A. Smalyuk, L. J. Atherton, L. R. Benedetti, R. Bionta, D. Bleuel, E. Bond, D. K. Bradley, J. Caggiano, D. A. Callahan, D. T. Casey, P. M. Celliers, C. J. Cerjan, D. Clark, E. L. Dewald, S. N. Dixit, T. Döppner, D. H. Edgell, M. J. Edwards, J. Frenje, M. Gatu-Johnson, V. Y. Glebov, S. Glenn, S. H. Glenzer, G. Grim, S. W. Haan, B. A. Hammel, E. Hartouni, R. Hatarik, S. Hatchett, D. G. Hicks, W. W. Hsing, N. Izumi, O. S. Jones, M. H. Key, S. F. Khan, J. D. Kilkenny, J. L. Kline, J. Knauer, G. A. Kyrala, O. L. Landen, S. Le Pape, J. D. Lindl, T. Ma, B. J. MacGowan, A. J. Mackinnon, A. G. MacPhee, J. McNaney, N. B. Meezan, J. D. Moody, A. Moore, M. Moran, E. I. Moses, A. Pak, T. Parham, H.-S. Park, P. K. Patel, R. Petrasso, J. E. Ralph, S. P. Regan, B. A. Remington, H. F. Robey, J. S. Ross, B. K. Spears, P. T. Springer, L. J. Suter, R. Tommasini, R. P. Town, S. V. Weber, and K. Widmann, Rev. Lett. **111**, 215001 (2013).
[6]M. J. Edwards, P. K. Patel, J. D. Lindl, L. J. Atherton, S. H. Glenzer, S. W. Haan, J. D. Kilkenny, O. L. Landen, E. I. Moses, A. Nikroo, R. Petrasso, T. C. Sangster, P. T. Springer, S. Batha, R. Benedetti, L. Bernstein, R. Betti, D. L. Bleuel, T. R. Boehly, D. K. Bradley, J. A. Caggiano, D. A. Callahan, P. M. Celliers, C. J. Cerjan, K. C. Chen, D. S. Clark, G. W. Collins, E. L. Dewald, L. Divol, S. Dixit, T. Döppner, D. H. Edgell, J. E. Fair, M. Farrell, R. J. Fortner, J. Frenje, M. G. Gatu Johnson, E. Giraldez, V. Yu. Glebov, G. Grim, B. A. Hammel, A. V. Hamza, D. R. Harding, S. P. Hatchett, N. Hein, H. W. Herrmann, D. Hicks, D. E. Hinkel, M. Hoppe, W. W. Hsing, N. Izumi, B. Jacoby, O. S. Jones, D. Kalantar, R. Kauffman, J. L. Kline, J. P. Knauer, J. A. Koch, B. J. Kozioziemski, G. Kyrala, K. N. LaFortune, S. Le Pape, R. J. Leeper, R. Lerche, T. Ma, B. J. MacGowan, A. J. MacKinnon, A. Macphee, E. R. Mapoles, M. M. Marinak, M. Mauldin, P. W. McKenty, M. Meezan, P. A. Michel, J. Milovich, J. D. Moody, M. Moran, D. H. Munro, C. L. Olson, K. Opachich, A. E. Pak, T. Parham, H.-S. Park, J. E. Ralph, S. P. Regan, B. Remington, H. Rinderknecht, H. F. Robey, M. Rosen, S. Ross, J. D. Salmonson, J. Sater, D. H. Schneider, F. H. Séguin, S. M. Sepke, D. A. Shaughnessy, V. A. Smalyuk, B. K. Spears, C. Stoeckl, W. Stoeffl, L. Suter, C. A. Thomas, R. Tommasini, R. P. Town, S. V. Weber, P. J. Wegner, K. Widman, M. Wilke, D. C. Wilson, C. B. Yeamans, and A. Zylstra, Phys. Plasmas **20**, 070501 (2013).
[7]S. W. Haan, J. D. Lindl, D. A. Callahan, D. S. Clark, J. D. Salmonson, B. A. Hammel, L. J. Atherton, R. C. Cook, M. J. Edwards, S. Glenzer, A. V. Hamza, S. P. Hatchett, M. C. Herrmann, D. E. Hinkel, D. D. Ho, H. Huang, O. S. Jones, J. Kline, G. Kyrala, O. L. Landen, B. J. Macgowan, M. M. Marinak, D. D. Meyerhofer, J. L. Milovich, K. A. Moreno, E. I. Moses, D. H. Munro, A. Nikroo, R. E. Olson, K. Peterson, S. M. Pollaine, J. E. Ralph, H. F. Robey, B. K. Spears, P. T. Springer, L. J. Suter, C. A. Thomas, R. P. Town, R. Vesey, S. V. Weber, H. L. Wilkens, and D. C. Wilson, Phys. Plasmas **18**, 051001 (2011).
[8]S. P. Regan, R. Epstein, B. A. Hammel, L. J. Suter, H. A. Scott, M. A. Barrios, D. K. Bradley, D. A. Callahan, C. Cerjan, G. W. Collins, S. N. Dixit, T. Döppner, M. J. Edwards, D. R. Farley, K. B. Fournier, S. Glenn, S. H. Glenzer, I. E. Golovkin, S. W. Haan, A. Hamza, D. G. Hicks, N. Izumi, O. S. Jones, J. D. Kilkenny, J. L. Kline, G. A. Kyrala, O. L. Landen, T. Ma, J. J. MacFarlane, A. J. MacKinnon, R. C. Mancini, R. L. McCrory, N. B. Meezan, D. D. Meyerhofer, A. Nikroo, H.-S. Park, J. Ralph, B. A. Remington, T. C. Sangster, V. A. Smalyuk, P. T. Springer, and R. P. J. Town, Phys. Rev. Lett. **111**, 045001 (2013).
[9]T. Ma, S. V. Weber, N. Izumi, P. T. Springer, P. K. Patel, M. H. Key, L. J. Atherton, L. R. Benedetti, D. K. Bradley, D. A. Callahan, P. M. Celliers, C. J. Cerjan, E. L. Dewald, S. N. Dixit, T. Döppner, D. H. Edgell, S. Glenn, G. Grim, S. W. Haan, B. A. Hammel, D. Hicks, W. W. Hsing, O. S. Jones, S. F. Khan, J. D. Kilkenny, J. L. Kline, G. A. Kyrala, O. L. Landen, S. Le Pape, B. J. MacGowan, A. J. Mackinnon, A. G. MacPhee, N. B. Meezan, J. D. Moody, A. Pak, T. Parham, H.-S. Park, J. E. Ralph, S. P. Regan, B. A. Remington, H. F. Robey, J. S. Ross, B. K. Spears, V. Smalyuk, L. J. Suter, R. Tommasini, R. P. Town, J. D. Lindl, M. J. Edwards, S. H. Glenzer, and E. I. Moses, Phys. Rev. Lett. **111**, 085004 (2013).
[10]R. D. Richtmyer, Commun. Pure Appl. Math. **13**, 297 (1960).
[11]E. E. Meshkov, Sov. Fluid Dyn. **4**, 101 (1969).
[12]Lord Rayleigh, Proc. London Math. Soc. **XIV**, 170 (1883).
[13]G. Taylor, Proc. R. Soc. London Ser. A **201**, 192 (1950).
[14]V. A. Smalyuk, S. V. Weber, D. T. Casey, D. S. Clark, J. E. Field, S. W. Haan, A. V. Hamza, D. E. Hoover, O. L. Landen, A. Nikroo, H. F. Robey, and C. R. Weber, High Power Laser Sci. Eng. **3**, e17 (2015).
[15]S. W. Haan, H. Huang, M. A. Johnson, M. Stadermann, S. Baxamusa, S. Bhandarkar, D. S. Clark, V. Smalyuk, and H. F. Robey, Phys. Plasmas **22**, 032708 (2015).
[16]V. A. Smalyuk, S. V. Weber, D. T. Casey, D. S. Clark, J. E. Field, S. W. Haan, B. A. Hammel, A. V. Hamza, D. E. Hoover, O. L. Landen, A. Nikroo, H. F. Robey, and C. R. Weber, Phys. Plasmas **22**, 072704 (2015).
[17]R. Tommasini, J. E. Field, B. A. Hammel, O. L. Landen, S. W. Haan, C. Aracne-Ruddle, L. R. Benedetti, D. K. Bradley, D. A. Callahan, E. L. Dewald, T. Doeppner, M. J. Edwards, O. A. Hurricane, N. Izumi, O. A. Jones, T. Ma, N. B. Meezan, S. R. Nagel, J. R. Rygg, K. S. Segraves, M. Stadermann, R. J. Strauser, and R. P. J. Town, Phys. Plasmas **22**, 056315 (2015).
[18]H.-S. Park, O. A. Hurricane, D. A. Callahan, D. T. Casey, E. L. Dewald, T. R. Dittrich, T. Döppner, D. E. Hinkel, L. F. B. Hopkins, S. Le Pape, T. Ma, P. K. Patel, B. A. Remington, H. F. Robey, J. D. Salmonson, and J. L. Kline, Phys. Rev. Lett. **112**, 055001 (2014).
[19]T. R. Dittrich, O. A. Hurricane, D. A. Callahan, E. L. Dewald, T. Döppner, D. E. Hinkel, L. F. Berzak Hopkins, S. Le Pape, T. Ma, J. L. Milovich, J. C. Moreno, P. K. Patel, H. S. Park, B. A. Remington, J. D. Salmonson, and J. L. Kline, Phys. Rev. Lett. **112**, 055002 (2014).
[20]O. A. Hurricane, D. A. Callahan, D. T. Casey, P. M. Celliers, C. Cerjan, E. L. Dewald, T. R. Dittrich, T. Doppner, D. E. Hinkel, L. F. B. Hopkins, J. L. Kline, S. Le Pape, T. Ma, A. G. MacPhee, J. L. Milovich, A. Pak, H. S.

Park, P. K. Patel, B. A. Remington, J. D. Salmonson, P. T. Springer, and R. Tommasini, Nature **506**(7488), 343–348 (2014).
[21]O. A. Hurricane, D. A. Callahan, D. T. Casey, E. L. Dewald, T. R. Dittrich, T. Döppner, M. A. Barrios Garcia, D. E. Hinkel, L. F. Berzak Hopkins, P. Kervin, J. L. Kline, S. Le Pape, T. Ma, A. G. MacPhee, J. L. Milovich, J. Moody, A. E. Pak, P. K. Patel, H.-S. Park, B. A. Remington, H. F. Robey, J. D. Salmonson, P. T. Springer, R. Tommasini, L. R. Benedetti, J. A. Caggiano, P. Celliers, C. Cerjan, R. Dylla-Spears, D. Edgell, M. J. Edwards, D. Fittinghoff, G. P. Grim, N. Guler, N. Izumi, J. A. Frenje, M. Gatu Johnson, S. Haan, R. Hatarik, H. Herrmann, S. Khan, J. Knauer, B. J. Kozioziemski, A. L. Kritcher, G. Kyrala, S. A. Maclaren, F. E. Merrill, P. Michel, J. Ralph, J. S. Ross, J. R. Rygg, M. B. Schneider, B. K. Spears, K. Widmann, and C. B. Yeamans, Phys. Plasmas **21**, 056314 (2014).
[22]T. Ma, O. A. Hurricane, D. A. Callahan, M. A. Barrios, D. T. Casey, E. L. Dewald, T. R. Dittrich, T. Döppner, S. W. Haan, D. E. Hinkel, L. F. Berzak Hopkins, S. Le Pape, A. G. MacPhee, A. Pak, H. S. Park, P. K. Patel, B. A. Remington, H. F. Robey, J. D. Salmonson, P. T. Springer, R. Tommasini, L. R. Benedetti, R. Bionta, E. Bond, D. K. Bradley, J. Caggiano, P. Celliers, C. J. Cerjan, J. A. Church, S. Dixit, R. Dylla-Spears, D. Edgell, M. J. Edwards, J. Field, D. N. Fittinghoff, J. A. Frenje, M. Gatu Johnson, G. Grim, N. Guler, R. Hatarik, H. W. Herrmann, W. W. Hsing, N. Izumi, O. S. Jones, S. F. Khan, J. D. Kilkenny, J. Knauer, T. Kohut, B. Kozioziemski, A. Kritcher, G. Kyrala, O. L. Landen, B. J. MacGowan, A. J. Mackinnon, N. B. Meezan, F. E. Merrill, J. D. Moody, S. R. Nagel, A. Nikroo, T. Parham, J. E. Ralph, M. D. Rosen, J. R. Rygg, J. Sater, D. Sayre, M. B. Schneider, D. Shaughnessy, B. K. Spears, R. P. J. Town, P. L. Volegov, A. Wan, K. Widmann, C. H. Wilde, and C. Yeamans, Phys. Rev. Lett. **114**, 145004 (2015).
[23]T. Döppner, D. A. Callahan, O. A. Hurricane, D. E. Hinkel, T. Ma, H. S. Park, L. F. Berzak Hopkins, D. T. Casey, P. Celliers, E. L. Dewald, T. R. Dittrich, S. W. Haan, A. L. Kritcher, A. MacPhee, S. Le Pape, A. Pak, P. K. Patel, P. T. Springer, J. D. Salmonson, R. Tommasini, L. R. Benedetti, E. Bond, D. K. Bradley, J. Caggiano, J. Church, S. Dixit, D. Edgell, M. J. Edwards, D. N. Fittinghoff, J. Frenje, M. Gatu Johnson, G. Grim, R. Hatarik, M. Havre, H. Herrmann, N. Izumi, S. F. Khan, J. L. Kline, J. Knauer, G. A. Kyrala, O. L. Landen, F. E. Merrill, J. Moody, A. S. Moore, A. Nikroo, J. E. Ralph, B. A. Remington, H. F. Robey, D. Sayre, M. Schneider, H. Streckert, R. Town, D. Turnbull, P. L. Volegov, A. Wan, K. Widmann, C. H. Wilde, and C. Yeamans, Phys. Rev. Lett. **115**, 055001 (2015).
[24]V. A. Smalyuk, J. A. Caggiano, D. T. Casey, C. J. Cerjan, D. S. Clark, M. J. Edwards, Grim, S. W. Haan, B. A. Hammel, A. Hamza, W. W. Hsing, O. Hurricane, J. D. Kilkenny, J. L. Kline, J. P. Knauer, O. L. Landen, J. M. McNaney, M. Mintz, A. Nikroo, T. Parham, H.-S. Park, J. Pino, K. Raman, B. A. Remington, H. F. Robey, D. P. Rowley, R. E. Tipton, S. V. Weber, and C. B. Yeamans, J. Phys.: Conference Series **688**, 012113 (2016).
[25]W. H. Goldstein, in Workshop on the Science of Fusion Ignition on NIF, San Ramon, CA, 22–24 May (2012).
[26]V. A. Smalyuk, D. T. Casey, D. S. Clark, M. J. Edwards, S. W. Haan, A. Hamza, D. E. Hoover, W. W. Hsing, O. Hurricane, J. D. Kilkenny, J. Kroll, O. L. Landen, A. Moore, A. Nikroo, A. Pak, J. L. Peterson, K. Raman, B. A. Remington, H. F. Robey, S. V. Weber, and K. Widmann, Phys. Rev. Lett. **112**, 185003 (2014).
[27]K. S. Raman, V. A. Smalyuk, D. T. Casey, S. W. Haan, D. E. Hoover, O. A. Hurricane, J. J. Kroll, A. Nikroo, J. L. Peterson, B. A. Remington, H. F. Robey, D. S. Clark, B. A. Hammel, O. L. Landen, M. Marinak, D. H. Munro, K. J. Peterson, and J. Salmonson, Phys. Plasmas **21**, 072710 (2014).
[28]D. T. Casey, V. A. Smalyuk, K. S. Raman, J. L. Peterson, L. Berzak Hopkins, D. A. Callahan, D. S. Clark, E. L. Dewald, T. R. Dittrich, S. W. Haan, D. E. Hinkel, D. Hoover, O. A. Hurricane, J. J. Kroll, O. L. Landen, A. S. Moore, A. Nikroo, H.-S. Park, B. A. Remington, H. F. Robey, J. R. Rygg, J. D. Salmonson, R. Tommasini, and K. Widmann, Phys. Rev. E **90**, 011102 (2014).
[29]V. A. Smalyuk, M. Barrios, J. A. Caggiano, D. T. Casey, C. J. Cerjan, D. S. Clark, M. J. Edwards, J. A. Frenje, M. Gatu-Johnson, V. Y. Glebov, G. Grim, S. W. Haan, B. A. Hammel, A. Hamza, D. E. Hoover, W. W. Hsing, O. Hurricane, J. D. Kilkenny, J. L. Kline, J. P. Knauer, J. Kroll, O. L. Landen, J. D. Lindl, T. Ma, J. M. McNaney, M. Mintz, A. Moore, A. Nikroo, T. Parham, J. L. Peterson, R. Petrasso, L. Pickworth, J. E. Pino, K. Raman, S. P. Regan, B. A. Remington, H. F. Robey, D. P. Rowley, D. B. Sayre, R. E. Tipton, S. V. Weber, K. Widmann, D. C. Wilson, and C. B. Yeamans, Phys. Plasmas **21**, 056301 (2014).
[30]J. L. Peterson, D. T. Casey, O. A. Hurricane, K. S. Raman, H. F. Robey, and V. A. Smalyuk, Phys. Plasmas **22**, 056309 (2015).
[31]D. S. Clark, J. L. Milovich, D. E. Hinkel, J. D. Salmonson, J. L. Peterson, L. F. Berzak Hopkins, D. C. Eder, S. W. Haan, O. S. Jones, M. M. Marinak, H. F. Robey, V. A. Smalyuk, and C. R. Weber, Phys. Plasmas **21**, 112705 (2014).
[32]J. L. Peterson, L. F. Berzak Hopkins, O. S. Jones, and D. S. Clark, Phys. Rev. E **91**, 031101(R) (2015).
[33]J. L. Milovich, H. F. Robey, D. S. Clark, K. L. Baker, D. A. Callahan, D. T. Casey, C. Cerjan, A. G. MacPhee, A. Pak, P. K. Patel, J. L. Peterson, V. A. Smalyuk, and C. R. Weber, Phys. Plasmas **22**, 122702 (2015).
[34]K. L. Baker, H. F. Robey, J. L. Milovich, V. A. Smalyuk, D. T. Casey, A. G. MacPhee, A. Pak, P. M. Celliers, D. S. Clark, O. L. Landen, J. L. Peterson, L. F. Berzak-Hopkins, C. R. Weber, S. W. Haan, T. D. Doppner, S. Dixit, E. Giraldez, A. V. Hamza, K. S. Jancaitis, J. J. Kroll, K. N. Lafortune, B. J. MacGowan, J. D. Moody, A. Nikroo, and C. C. Widmayer, Phys. Plasmas **22**, 052702 (2015).
[35]A. G. MacPhee, D. T. Casey, D. S. Clark, O. S. Jones, J. L. Milovich, J. L. Peterson, H. F. Robey, and V. A. Smalyuk, Phys. Plasmas **22**, 080702 (2015).
[36]D. T. Casey, J. Milovich, V. Smalyuk, D. Clark, H. Robey, A. Pak, A. MacPhee, K. Baker, T. Ma, H.-S. Park, T. Döppner, D. Callahan, S. Haan, L. Peterson, P. Patel, A. Hamza, O. Jones, C. Weber, D. Hoover, A. Nikroo, C. Yeamans, F. Merrill, P. L. Volegov, D. Fittinghoff, G. Grim, S. Nagel, R. Benedetti, N. Izumi, J. Edwards, O. Landen, S. Khan, K. N. Lafortune, B. J. MacGowan, C. C. Widmayer, D. Sayre, R. Hatarik, E. Bond, C. Cerjan, M. Gatu Johnson, J. Frenje, and D. Edgell, Phys. Rev. Lett. **115**, 105001 (2015).
[37]V. A. Smalyuk, H. F. Robey, T. Döppner, O. S. Jones, J. L. Milovich, B. Bachmann, K. L. Baker, L. F. Berzak-Hopkins, E. Bond, D. A. Callahan, D. T. Casey, P. M. Celliers, C. Cerjan, D. S. Clark, S. N. Dixit, M. J. Edwards, E. Giraldez, S. W. Haan, A. V. Hamza, M. Hohenberger, D. Hoover, O. A. Hurricane, K. S. Jancaitis, J. J. Kroll, K. N. Lafortune, O. L. Landen, B. J. MacGowan, A. G. MacPhee, A. Nikroo, A. Pak, P. K. Patel, J. L. Peterson, C. R. Weber, C. C. Widmayer, and C. Yeamans, Phys. Plasmas **22**, 080703 (2015).
[38]H. F. Robey, V. A. Smalyuk, J. L. Milovich, T. Döppner, D. T. Casey, K. L. Baker, J. L. Peterson, B. Bachmann, L. F. Berzak Hopkins, E. Bond, J. A. Caggiano, D. A. Callahan, P. M. Celliers, C. Cerjan, D. S. Clark, S. N. Dixit, M. J. Edwards, N. Gharibyan, S. W. Haan, B. A. Hammel, A. V. Hamza, R. Hatarik, O. A. Hurricane, K. S. Jancaitis, O. S. Jones, G. D. Kerbel, J. J. Kroll, K. N. Lafortune, O. L. Landen, T. Ma, M. M. Marinak, B. J. MacGowan, A. G. MacPhee, A. Pak, M. Patel, P. K. Patel, L. J. Perkins, D. B. Sayre, S. M. Sepke, B. K. Spears, R. Tommasini, C. R. Weber, C. C. Widmayer, C. Yeamans, E. Giraldez, D. Hoover, A. Nikroo, M. Hohenberger, and M. Gatu Johnson, Phys. Plasmas **23**, 056303 (2016).
[39]J. L. Kline, K. Widmann, A. Warrick, R. E. Olson, C. A. Thomas, A. S. Moore, L. J. Suter, O. Landen, D. Callahan, S. Azevedo, J. Liebman, S. H. Glenzer, A. Conder, S. N. Dixit, P. Torres III, V. Tran, E. L. Dewald, J. Kamperschroer, L. J. Atherton, R. Beeler, Jr., L. Berzins, J. Celeste, C. Haynam, W. Hsing, D. Larson, B. J. MacGowan, D. Hinkel, D. Kalantar, R. Kauffman, J. Kilkenny, N. Meezan, M. D. Rosen, M. Schneider, E. A. Williams, S. Vernon, R. J. Wallace, B. Van Wonterghem, and B. K. Young, Rev. Sci. Instrum. **81**, 10E321 (2010).
[40]S. E. Bodner, D. G. Colombant, J. H. Gardner, R. H. Lehmberg, R. L. McCrory, W. Seka, C. P. Verdon, J. P., Knauer, B. B., Afeyan, and H. T. Powell, Phys. Plasmas **5**, 1901 (1998).
[41]V. N. Goncharov, J. P. Knauer, P. W. McKenty, P. B. Radha, T. C. Sangster, S. Skupsky, R. Betti, R. L. McCrory, and D. D. Meyerhofer, Phys. Plasmas **10**, 1906 (2003).
[42]K. Anderson and R. Betti, Phys. Plasmas **10**, 4448 (2003).
[43]R. Betti, K. Anderson, J. Knauer, T. J. B. Collins, R. L. McCrory, P. W. McKenty, and S. Skupsky, Phys. Plasmas **12**, 042703 (2005).
[44]V. A. Smalyuk, V. N. Goncharov, K. S. Anderson, R. Betti, R. S. Craxton, J. A. Delettrez, D. D. Meyerhofer, S. P. Regan, and T. C. Sangster, Phys. Plasmas **14**, 032702 (2007).
[45]N. Metzler, A. L. Velikovich, and J. H. Gardner, Phys. Plasmas **6**, 3283 (1999).
[46]V. N. Goncharov, Phys. Rev. Lett. **82**, 2091 (1999).
[47]Y. Aglitskiy, A. L. Velikovich, M. Karasik, V. Serlin, C. J. Pawley, A. J. Schmitt, S. P. Obenschain, A. N. Mostovych, J. H. Gardner, and N. Metzler, Phys. Rev. Lett. **87**, 265001 (2001).

[48]O. V. Gotchev, V. N. Goncharov, J. P. Knauer, T. R. Boehly, T. J. B. Collins, R. Epstein, P. A. Jaanimagi, and D. D. Meyerhofer, Phys. Rev. Lett. **96**, 115005 (2006).
[49]V. N. Goncharov, O. V. Gotchev, E. Vianello, T. R. Boehly, J. P. Knauer, P. W. McKenty, P. B. Radha, S. P. Regan, T. C. Sangster, S. Skupsky, V. A. Smalyuk, R. Betti, R. L. McCrory, D. D. Meyerhofer, and C. Cherfils-Clérouin, Phys. Plasmas **13**, 012702 (2006).
[50]A. L. Velikovich, F. L. Cochran, and J. Davis, Phys. Rev. Lett. **77**, 853 (1996).
[51]J. L. Peterson, D. S. Clark, L. P. Masse, and L. J. Suter, Phys. Plasmas **21**, 092710 (2014).
[52]O. L. Landen, K. L. Baker, D. S. Clark, V. N. Goncharov, B. A. Hammel, D. D. Ho, O. A. Hurricane, J. D. Lindl, E. N. Loomis, L. Masse, C. Mauche, J. L. Milovich, J. L. Peterson, V. A. Smalyuk, S. A. Yi, A. L. Velikovich, and C. Weber, J. Phys. Conf. Ser. **717**, 012034 (2016).
[53]M. G. Johnson, J. A. Frenje, D. T. Casey, C. K. Li, F. H. Seguin, R. Petrasso, R. Ashabranner, R. M. Bionta, D. L. Bleuel, E. J. Bond, J. A. Caggiano, A. Carpenter, C. J. Cerjan, T. J. Clancy, T. Doeppner, M. J. Eckart, M. J. Edwards, S. Friedrich, S. H. Glenzer, S. W. Haan, E. P. Hartouni, R. Hatarik, S. P. Hatchett, O. S. Jones, G. Kyrala, S. L. Pape, R. A. Lerche, O. L. Landen, T. Ma, A. J. MacKinnon, M. A. McKernan, M. J. Moran, E. Moses, D. H. Munro, J. McNaney, H. S. Park, J. Ralph, B. Remington, J. R. Rygg, S. M. Sepke, V. Smalyuk, B. Spears, P. T. Springer, C. B. Yeamans, M. Farrell, D. Jasion, J. D. Kilkenny, A. Nikroo, R. Paguio, J. P. Knauer, V. Y. Glebov, T. C. Sangster, R. Betti, C. Stoeckl, J. Magoon, M. J. Shoup III, G. P. Grim, J. Kline, G. L. Morgan, T. J. Murphy, R. J. Leeper, C. L. Ruiz, G. W. Cooper, and A. J. Nelson, Rev. Sc. Instrum. **83**, 10D308 (2012).
[54]T. Ma, N. Izumi, R. Tommasini, D. K. Bradley, P. Bell, C. J. Cerjan, S. Dixit, T. Döppner, O. Jones, J. L. Kline, G. Kyrala, O. L. Landen, S. LePape, A. J. Mackinnon, H.-S. Park, P. K. Patel, R. R. Prasad, J. Ralph, S. P. Regan, V. A. Smalyuk, P. T. Springer, L. Suter, R. P. J. Town, S. V. Weber, and S. H. Glenzer, Rev. Sci. Instrum. **83**, 10E115 (2012).
[55]G. P. Grim, N. Guler, F. E. Merrill, G. L. Morgan, C. R. Danly, P. L. Volegov, C. H. Wilde, D. C. Wilson, D. S. Clark, D. E. Hinkel, O. S. Jones, K. S. Raman, N. Izumi, D. N. Fittinghoff, O. B. Drury, E. T. Alger, P. A. Arnold, R. C. Ashabranner, L. J. Atherton, M. A. Barrios, S. Batha, P. M. Bell, L. R. Benedetti, R. L. Berger, L. A. Bernstein, L. V. Berzins, R. Betti, S. D. Bhandarkar, R. M. Bionta, D. L. Bleuel, T. R. Boehly, E. J. Bond, M. W. Bowers, D. K. Bradley, G. K. Brunton, R. A. Buckles, S. C. Burkhart, R. F. Burr, J. A. Caggiano, D. A. Callahan, D. T. Casey, C. Castro, P. M. Celliers, C. J. Cerjan, G. A. Chandler, C. Choate, S. J. Cohen, G. W. Collins, G. W. Cooper, J. R. Cox, J. R. Cradick, P. S. Datte, E. L. Dewald, P. D. Nicola, J. M. D. Nicola, L. Divol, S. N. Dixit, R. Dylla-Spears, E. G. Dzenitis, M. J. Eckart, D. C. Eder, D. H. Edgell, M. J. Edwards, J. H. Eggert, R. B. Ehrlich, G. V. Erbert, J. Fair, D. R. Farley, B. Felker, R. J. Fortner, J. A. Frenje, G. Frieders, S. Friedrich, M. Gatu-Johnson, C. R. Gibson, E. Giraldez, V. Y. Glebov, S. M. Glenn, S. H. Glenzer, G. Gururangan, S. W. Haan, K. D. Hahn, B. A. Hammel, A. V. Hamza, E. P. Hartouni, R. Hatarik, S. P. Hatchett, C. Haynam, M. R. Hermann, H. W. Herrmann, D. G. Hicks, J. P. Holder, D. M. Holunga, J. B. Horner, W. W. Hsing, H. Huang, M. C. Jackson, K. S. Jancaitis, D. H. Kalantar, R. L. Kauffman, M. I. Kauffman, S. F. Khan, J. D. Kilkenny, J. R. Kimbrough, R. Kirkwood, J. L. Kline, J. P. Knauer, K. M. Knittel, J. A. Koch, T. R. Kohut, B. J. Kozioziemski, K. Krauter, G. W. Krauter, A. L. Kritcher, J. Kroll, G. A. Kyrala, K. N. L. Fortune, G. LaCaille, L. J. Lagin, T. A. Land, O. L. Landen, D. W. Larson, D. A. Latray, R. J. Leeper, T. L. Lewis, S. LePape, J. D. Lindl, R. R. Lowe-Webb, T. Ma, B. J. MacGowan, A. J. MacKinnon, A. G. MacPhee, R. M. Malone, T. N. Malsbury, E. Mapoles, C. D. Marshall, D. G. Mathisen, P. McKenty, J. M. McNaney, N. B. Meezan, P. Michel, J. L. Milovich, J. D. Moody, A. S. Moore, M. J. Moran, K. Moreno, E. I. Moses, D. H. Munro, B. R. Nathan, A. J. Nelson, A. Nikroo, R. E. Olson, C. Orth, A. E. Pak, E. S. Palma, T. G. Parham, P. K. Patel, R. W. Patterson, R. D. Petrasso, R. Prasad, J. E. Ralph, S. P. Regan, H. Rinderknecht, H. F. Robey, G. F. Ross, C. L. Ruiz, F. H. Seguin, J. D. Salmonson, T. C. Sangster, J. D. Sater, R. L. Saunders, M. B. Schneider, D. H. Schneider, M. J. Shaw, N. Simanovskaia, B. K. Spears, P. T. Springer, C. Stoeckl, W. Stoeffl, L. J. Suter, C. A. Thomas, R. Tommasini, R. P. Town, A. J. Traille, B. V. Wonterghem, R. J. Wallace, S. Weaver, S. V. Weber, P. J. Wegner, P. K. Whitman, K. Widmann, C. C. Widmayer, R. D. Wood, B. K. Young, R. A. Zacharias, and A. Zylstra, Phys. Plasmas **20**, 056320 (2013).
[56]R. Hatarik, D. B. Sayre, J. A. Caggiano, T. Phillips, M. J. Eckart, E. J. Bond, C. Cerjan, G. P. Grim, E. P. Hartouni, J. P. Knauer, J. M. Mcnaney, and D. H. Munro, J. Appl. Phys. **118**, 184502 (2015).
[57]D. A. Shaughnessy, K. J. Moody, N. Gharibyan, P. M. Grant, J. M. Gostic, P. C. Torretto, P. T. Wooddy, B. B. Bandong, J. D. Despotopulos, C. J. Cerjan, C. A. Hagmann, J. A. Caggiano, C. B. Yeamans, L. A. Bernstein, D. H. G. Schneider, E. A. Henry, and R. J. Fortner, Rev. Sci. Instrum. **85**, 063508 (2014).
[58]C. Hagmann, D. A. Shaughnessy, K. J. Moody, P. M. Grant, N. Gharibyan, J. M. Gostic, P. T. Wooddy, P. C. Torretto, B. B. Bandong, R. Bionta, C. J. Cerjan, L. A. Bernstein, J. A. Caggiano, H. W. Herrmann, J. P. Knauer, D. B. Sayre, D. H. Schneider, E. A. Henry, and R. J. Fortner, Rev. Sci. Instrum. **86**, 076105 (2015).
[59]D. L. Bleuel, C. B. Yeamans, L. A. Bernstein, R. M. Bionta, J. A. Caggiano, D. T. Casey, G. W. Cooper, O. B. Drury, J. A. Frenje, C. A. Hagmann, R. Hatarik, J. P. Knauer, M. G. Johnson, K. M. Knittel, R. J. Leeper, J. M. McNaney, M. Moran, C. L. Ruiz, and D. H. G. Schneider, Rev. Sci. Instrum. **83**(10), 10D313 (2012).
[60]T. Döppner, B. Bachmann, F. Albert, P. Bell, S. Burns, J. Celeste, R. Chow, L. Divol, E. L. Deward, M. Hohenberger, C. Huntington, N. Izumi, G. LaCaille, O. L. Landen, N. Palmer, H.-S. Park, and C. A. Thomas, J. Inst. **11**, P06010 (2016).
[61]O. L. Landen, private communication (2016).
[62]V. N. Goncharov, T. C. Sangster, R. Betti, T. R. Boehly, M. J. Bonino, T. J. B. Collins, R. S. Craxton, J. A. Delettrez, D. H. Edgell, R. Epstein, R. K. Follett, C. J. Forrest, D. H. Froula, V. Yu. Glebov, D. R. Harding, R. J. Henchen, S. X. Hu, I. V. Igumenshchev, R. Janezic, J. H. Kelly, T. J. Kessler, T. Z. Kosc, S. J. Loucks, J. A. Marozas, F. J. Marshall, A. V. Maximov, R. L. McCrory, P. W. McKenty, D. D. Meyerhofer, D. T. Michel, J. F. Myatt, R. Nora, P. B. Radha, S. P. Regan, W. Seka, W. T. Shmayda, R. W. Short, A. Shvydky, S. Skupsky, C. Stoeckl, B. Yaakobi, J. A. Frenje, M. Gatu-Johnson, R. D. Petrasso, and D. T. Casey, Phys. Plasmas **21**, 056315 (2014).
[63]R. Betti, P. Y. Chang, B. K. Spears, K. S. Anderson, J. Edwards, M. Fatenejad, J. D. Lindl, R. L. McCrory, R. Nora, and D. Shvarts, Phys. Plasmas **17**, 058102 (2010).
[64]D. S. Clark, C. R. Weber, J. L. Milovich, J. D. Salmonson, A. L. Kritcher, S. W. Haan, B. A. Hammel, D. E. Hinkel, O. A. Hurricane, O. S. Jones, M. M. Marinak, P. K. Patel, H. F. Robey, S. M. Sepke, and M. J. Edwards, Phys. Plasmas **23**, 056302 (2016).
[65]D. S. Clark, C. R. Weber, V. A. Smalyuk, H. F. Robey, A. L. Kritcher, J. L. Milovich, and J. D. Salmonson, Phys. Plasmas **23**, 072707 (2016).
[66]J. Gu, Z. Dai, P. Song, S. Zou, W. Ye, W. Zheng, P. Gu, J. Wang, and S. Zhu, Phys. Plasmas **23**, 082703 (2016).
[67]J. D. Lindl, O. L. Landen, J. Edwards, E. I. Moses, J. Adams, P. A. Amendt, N. Antipa, P. A. Arnold, L. J. Atherton, S. Azevedo, D. Barker, M. A. Barrios, I. Bass, S. H. Baxamusa, R. Beeler, B. V. Beeman, P. M. Bell, L. R. Benedetti, L. Bernstein, L. Berzak Hopkins, S. D. Bhandarkar, T. Biesiada, R. M. Bionta, D. L. Bleuel, E. J. Bond, M. Borden, M. W. Bowers, D. K. Bradley, D. Browning, G. K. Brunton, J. Bude, S. C. Burkhart, R. F. Burr, B. Butlin, J. A. Caggiano, D. A. Callahan, A. C. Carpenter, C. W. Carr, D. T. Casey, C. Castro, J. Celeste, P. M. Celliers, C. J. Cerjan, J. Chang, M. Chiarappa-Zucca, C. Choate, T. J. Clancy, D. S. Clark, S. J. Cohen, G. W. Collins, A. Conder, J. R. Cox, P. S. Datte, G. A. Deis, E. L. Dewald, P. Di Nicola, J. M. Di Nicola, L. Divol, S. N. Dixit, T. Döppner, V. Draggoo, O. Drury, R. Dylla-Spears, E. G. Dzenitis, J. M. Dzenitis, M. J. Eckart, D. C. Eder, J. H. Eggert, R. B. Ehrlich, G. V. Erbert, J. Fair, D. R. Farley, M. Fedorov, B. Felker, R. Finucane, A. Fisher, D. N. Fittinghoff, J. Folta, R. J. Fortner, T. Frazier, G. Frieders, S. Frieders, S. Friedrich, J. Fry, J. Gaylord, S. M. Glenn, S. H. Glenzer, B. Golick, G. Gururangan, G. Guss, S. W. Haan, B. J. Haid, B. Hammel, A. V. Hamza, E. P. Hartouni, R. Hatarik, B. W. Hatch, S. P. Hatchett, R. Hawley, C. Haynam, J. Heebner, G. Heestand, M. R. Hermann, V. J. Hernandez, D. G. Hicks, D. E. Hinkel, D. D. Ho, J. P. Holder, D. Holunga, J. Honig, J. Horner, R. K. House, M. Hutton, N. Izumi, M. C. Jackson, K. S. Jancaitis, D. R. Jedlovec, M. A. Johnson, O. S. Jones, D. H. Kalantar, R. L. Kauffman, L. Kegelmeyer, G. Kerbel, M. Key, S. F. Khan, J. R. Kimbrough, R. Kirkwood, J. J. Klingman, J. A. Koch, T. R. Kohut, J. M. Koning, K. M. Knittel, B. J. Kozioziemski, G. W. Krauter, K. Krauter, A. Kritcher, J. Kroll, W. L. Kruer, G. LaCaille, K. N. LaFortune, L. J. Lagin, T. A. Land, A. B. Langdon, S. H. Langer, D. W. Larson, D. A. Latray, T. Laurence, S. LePape, R. A. Lerche, Z. Liao, J. Liebman, R. A. London, R. R. Lowe-Webb, T. Ma, B. J. MacGowan, A. J. MacKinnon, A. G. MacPhee, T. N. Malsbury, K. Manes, A. M. Manuel, E. R. Mapoles, M.

M. Marinak, C. D. Marshall, D. Mason, N. Masters, D. G. Mathisen, I. Matthews, T. McCarville, J. M. McNaney, D. J. Meeker, N. B. Meezan, J. Menapace, P. Michel, P. E. Miller, J. L. Milovich, M. Mintz, R. Montesanti, M. Monticelli, J. D. Moody, M. J. Moran, J. C. Moreno, D. H. Munro, R. A. Negres, J. R. Nelson, M. Norton, M. Nostrand, M. Brien, Y. P. Opachich, C. Orth, A. E. Pak, E. S. Palma, J. N. E. Palmer, T. G. Parham, H.-S. Park, P. K. Patel, R. W. Patterson, J. E. Peterson, J. L. Peterson, T. Phillips, R. Prasad, K. Primdahl, S. T. Prisbrey, S. R. Qiu, J. E. Ralph, K. S. Raman, F. Ravizza, B. Raymond, B. A. Remington, M. A. Rever, J. Reynolds, M. J. Richardson, A. C. Riddle, B. Rittmann, M. D. Rosen, J. S. Ross, J. R. Rygg, R. A. Sacks, J. T. Salmon, J. D. Salmonson, J. D. Sater, R. L. Saunders, R. Sawicki, K. Schaffers, D. H. Schneider, M. B. Schneider, H. A. Scott, S. M. Sepke, R. Seugling, D. A. Shaughnessy, M. J. Shaw, R. Shelton, N. Shen, N. Shingleton, N. Simanovskaia, V. Smalyuk, D. A. Smauley, M. Spaeth, B. K. Spears, D. R. Speck, T. M. Spinka, P. T. Springer, M. Stadermann, W. Stoeffl, J. Stolken, C. Stolz, E. Storm, D. J. Strozzi, T. Suratwala, L. J. Suter, J. S. Taylor, C. A. Thomas, G. L. Tietbohl, R. Tommasini, D. Trummer, B. VanWonterghem, R. Von Rotz, R. J. Wallace, C. F. Walters, A. Wang, A. L. Warrick, S. Weaver, S. V. Weber, P. J. Wegner, K. Widmann, C. C. Widmayer, E. A. Williams, P. K. Whitman, K. Wilhelmsen, M. Witte, L. Wong, R. D. Wood, S. Yang, C. Yeamans, B. K. Young, B. Yoxall, R. A. Zacharias, G. B. Zimmerman, S. Batha, C. R. Danly, V. Fatherley, G. P. Grim, N. Guler, H. W. Herrmann, Y. Kim, J. L. Kline, G. A. Kyrala, R. J. Leeper, D. Martinson, F. E. Merrill, R. E. Olson, C. Wilde, M. D. Wilke, D. C. Wilson, G. A. Chandler, G. W. Cooper, K. D. Hahn, K. J. Peterson, C. L. Ruiz, K. C. Chen, N. Dorsano, M. Emerich, C. Gibson, D. Hoover, M. Hoppe, J. D. Kilkenny, K. Moreno, H. Wilkens, S. Woods, J. A. Frenje, M. G. Johnson, C. K. Li, R. D. Petrasso, H. Rinderknecht, M. Rosenberg, F. H. Séguin, A. Zylstra, W. Garbett, P. Graham, T. Guymer, A. S. Moore, J.-L. Bourgade, P. Gauthier, J.-P. Leidinger, L. Masse, F. Philippe, and R. H. H. Scott, Phys. Plasmas **21**, 129902 (2014).

[68]B. K. Spears, S. Glenzer, M. J. Edwards, S. Brandon, D. Clark, R. Town, C. Cerjan, R. Dylla-Spears, E. Mapoles, D. Munro, J. Salmonson, S. Sepke, S. Weber, S. Hatchett, S. Haan, P. Springer, E. Moses, J. Kline, G. Kyrala, and D. Wilson, Phys. Plasmas **19**, 056316 (2012).

[69]B. K. Spears, S. Brandon, D. Clark, C. Cerjan, J. Edwards, O. Landen, J. Lindl, S. Haan, S. Hatchett, J. Salmonson, P. Springer, S. V. Weber, and D. Wilson, J. Phys. Conf. Ser. **244**, 022014 (2010).

[70]R. Betti, A. R. Christopherson, B. K. Spears, R. Nora, A. Bose, J. Howard, K. M. Woo, M. J. Edwards, and J. Sanz, Phys. Rev. Lett. **114**, 255003 (2015).